

Monitoring and Evaluation of Alabama's First Geosynthetic Reinforced Soil-Integrated Bridge System

by

R. Jonathan Hogan

A thesis submitted to the Graduate Faculty of
Auburn University
in partial fulfillment of the
requirements for the Degree of
Master of Science

Auburn, Alabama
December 15, 2018

Keywords: GRS-IBS, instrumentation, reinforced backfill, geosynthetics

Copyright 2018 by R. Jonathan Hogan

Approved by

Jack Montgomery, Ph.D., Chair, Assistant Professor of Civil Engineering
J. Brian Anderson, Ph.D., P.E., Co-Chair, Associate Professor of Civil Engineering
Anton Schindler, Ph.D., P.E. Associate Professor Civil Engineering

ABSTRACT

Geosynthetic reinforced soil-integrated bridge systems (GRS-IBS) use closely spaced layers of geosynthetic reinforcement and compacted granular backfill to directly support the bridge deck and blend the abutment and roadway approach for a smooth transition. These systems are designed for areas where a single span is sufficient to bridge over a gap in the roadway. GRS-IBS structures have been successfully implemented in many states. Alabama has recently completed its first GRS-IBS in Marshall County, which is located within the Sand Mountain region of the Appalachian Plateau. The robust mechanical properties of the native material provided a good location to construct the first GRS-IBS in Alabama due to the low risk of scour and excessive settlement. Two 12-ft tall by 33-ft wide GRS abutments were constructed to support the load of seven, 1.75-ft thick by 4-ft wide by 52-ft long, reinforced concrete box beams, pavement and traffic. Construction of the GRS abutments was completed in three phases: excavation of the native sandstone, forming and placement of the concrete foundation, and placement of the segmental retaining wall (SRW) masonry units and reinforced backfill.

The bridge beams and integrated approach were placed after the GRS structure was completed. The integrated approach consists of four layers of biaxially woven geosynthetic wrapped around No. 89 gravel, a final layer of woven geosynthetic wrapped around dense grade base and covered with asphalt pavement. Earth and pore pressure instruments were placed within the first and second layers of the two GRS abutments. Since construction began, data have indicated that earth-pressures have increased to 1800-psf after placement of the bridge beams, while pore-pressures

have remained near zero. Surveys of the abutment have shown no significant movement since completion of construction. These results indicate that the bridge is performing as expected.

ACKNOWLEDGMENTS

I would like to thank the Alabama Department of Transportation and Robert Pirando, P.E. for their support of this research project. I would also like to thank Dr. Jack Montgomery and Dr. J. Brian Anderson for their support and guidance during my time as a graduate student at Auburn University and helping me find a job with a great company. Furthermore, I would like to thank Dr. Anton Schindler for providing me with insight into the mechanics of concrete materials and willingness to join my committee on short notice. I would also like to thank the following people for their work on this project: Chao Shi, Michael Kiernan, Lydia Kennedy, and Samuel Dunlop. Finally, I would like to thank my family for their insight and support during my time at Auburn University. Above all, I would like thank God for providing me with the skills and ability to complete this achievement.

TABLE OF CONTENTS

Abstract	ii
Acknowledgments.....	iv
Table of Contents	v
List of Tables	viii
List of Figures	ix
List of Abbreviations and Symbols.....	xii
Chapter 1: Introduction.....	1
1.1 Overview.....	1
1.2 Objective	3
1.3 Scope.....	3
Chapter 2: Background and Literature Review	5
2.1 Overview of GRS-IBS Technology.....	5
2.2 Design Approach	16
2.2.1 Global Failure Modes	22
2.2.2 Ultimate Capacity	23
2.2.3 In-Service Strains.....	25
2.2.4 Reinforcement Strength and spacing	26
2.3 Performance of Selected Bridges.....	27
Chapter 3: Design of the Marshall County GRS-IBS.....	29
3.1 Site Description.....	29

3.2	Site Geology.....	30
3.3	Design	31
3.4	Materials	33
Chapter 4: Construction Process.....		38
4.1	Demolition and Excavation.....	38
4.2	Concrete Foundation.....	39
4.3	GRS Abutment.....	39
4.4	Beam Placement.....	41
4.5	Final Grading and Paving	43
4.6	Construction Issues	43
Chapter 5: Instrumentation		45
5.1	Time-lapse Cameras.....	45
5.2	Pore-Pressure Sensors	46
5.3	Earth-Pressure Cells.....	50
5.4	Data Loggers	52
5.5	Survey Instrument and Targets	54
Chapter 6: Results and discussion.....		56
6.1	Earth-Pressure Measurements.....	56
6.2	Pore-Pressure Readings	57
6.3	Geospatial Monitoring	58
6.3.1	Settlement	58
6.3.2	Lateral Displacement	61
Chapter 7: Summary, Conclusions, and Recommendations.....		64

7.1	Summary of the Project	64
7.2	Image Recording.....	64
7.2.1	Summary	64
7.2.2	Conclusions.....	65
7.3	Geospatial Monitoring	65
7.3.1	Summary	65
7.3.2	Conclusions.....	65
7.4	Instrumentation	67
7.4.1	Summary	67
7.4.2	Conclusions.....	67
7.5	Recommendations.....	68
	References.....	70

LIST OF TABLES

Table 1: Selected well and open-graded aggregate specifications (after Adams et al. 2011a).	9
Table 2: Standardized test methods used for geosynthetics in GRS-IBS	16
Table 3: Calculated bearing and sliding factors of safety and volume of rock excavation (after Elton 2014).....	32
Table 4. No. 89 stone gradation results (after from ALDOT 2017)	34
Table 5. Selected tensile strength measurements of the 4800 geosynthetic (after from SGI Testing Services, LLC 2017)	35
Table 6. Selected test results (ASTM C140-16 and ASTM C1372-16) of segmental retaining wall masonry units (after S&ME 2017).....	35

LIST OF FIGURES

Figure 1: Olympic Avenue GRS abutment in Buchanan County, Iowa. Abutments use grouted riprap over wrapped geosynthetic face for scour protection (photo from Vennapusa et al. 2012).	2
Figure 2: Placing prestressed concrete box beams onto the beam seat of the Marshall County GRS with segmental retaining wall (SRW) unit facing.....	3
Figure 3: Typical cross section of GRS-IBS (Adams et al. 2011a).....	6
Figure 4: Performance test results of vertical strain with applied load with and without a facing material. The geosynthetic reinforcement was spaced at 11.25-in. with a tensile strength of 3,600 lb/ft (Nicks et al. 2013).....	8
Figure 5: Scour locations near bridge abutments (Ghazvinei et al. 2014).....	11
Figure 6: Biaxial woven polypropylene (PP) geosynthetic with rule for scale	12
Figure 7: Uniaxial and biaxial geogrids on the left and right respectively (Shukla 2002).....	12
Figure 8: Uniaxial geosynthetic and soil particles interlocked within the aperture space (Shukla 2002).....	13
Figure 9: Geosynthetic material placed within soil mass under tension (after Shukla 1992). 14	
Figure 10: Direction nomenclature for geosynthetic materials (igeosynthetics 2017).....	16
Figure 11: Equivalent stress loads and resultant lateral stresses considered in the design of GRS-IBS: a.) the GRS structure with all DLs and LLs applied at the surface of the abutment and integrated approach, b.) superposition of the lateral stress distributions due to the weight of reinforced backfill, bridge DLs and LLs, and c.) lateral stress distributions due to all vertical loads applied at surface (after Adams et al. 2011a).....	19
Figure 12: Boussinesq lateral stress in retaining structure due to distributed load at the surface (after from Adams et al. 2011a).	20
Figure 13: Stress-strain performance design envelopes for vertical capacity, using different compacted reinforced backfills (Adams et al. 2011b).	25
Figure 14: Location of GRS-IBS construction site.....	30
Figure 15: Generalized stratigraphy of GRS-IBS construction site (ALDOT 2017)	31

Figure 16. Design profile of GRS-IBS in Albertville, AL (after from ALDOT 2017). 33

Figure 17. (a) Selected woven geosynthetic; (b) segmental retaining wall masonry units..... 34

Figure 18: Mohr-Coulomb failure criteria for No. 89 backfill. 36

Figure 19: Stress-strain behavior for No. 89 backfill material. 37

Figure 20: (a) Removal of the existing bridge at Turkey Creek; (b) removal of blasted sandstone, on the western side of Turkey Creek..... 38

Figure 21: (a) Leveling form boards in the excavation for placement of the concrete pad; (b) Concrete being placed using a concrete bucket suspended from a hydraulic excavator. 39

Figure 22: (a) Placement of initial layer of No. 89 stone to top of first row of masonry blocks and (b) placement of geosynthetic and second row of masonry blocks. 40

Figure 23: The finished GRS abutment prior to placement of the bridge beams. 41

Figure 24: Bridge beam setting on top of CMU with 3 in. gap between abutment and beam and integrated approach reinforcement layer. The circular opening for post-tensioning can be seen at the end of the beam. 42

Figure 25: Placed bridge beams and the integrated approach..... 42

Figure 26: The completed GRS-IBS over Turkey Creek in Marshall County, AL. 43

Figure 27: Wingscapes time-lapse camera used for the project, right photo shows the programming panel on the inside of the cover (Wingscapes 2015)..... 46

Figure 28: Model 4500 standard vibrating wire piezometer (Geokon 2017) 47

Figure 29: Internal components of vibrating wire sensor (Geokon 2017)..... 48

Figure 30: Plan view of the layout of the sensors and survey targets used on the GRS-IBS structure..... 49

Figure 31: Sensor cables routed through chiseled openings in the SRW units. 50

Figure 32: Model 4810 contact pressure cell (Geokon 2017)..... 51

Figure 33: Installed earth and pore pressure sensors covered with sand to mitigate arching. 52

Figure 34: CRVW-3 data logger used for project (Campbell Scientific 2018) 53

Figure 35: Topcon GTS-235W total station 54

Figure 36: RS60 survey target mounted onto a GRS abutment..... 55

Figure 37: Earth pressure sensor readings show the increase in earth pressure as load is applied in the east and west abutments 57

Figure 38. Pore pressure sensor readings for the east and west abutments 58

Figure 39: Settlement measurements of the northeast corner of the east abutment..... 60

Figure 40: Settlement measurements of the southeast corner of the east abutment. 60

Figure 41: Settlement measurements of the southwest corner of the west abutment. 61

Figure 42: Settlement measurements of the northwest corner of the west abutment. 61

Figure 43: Measured lateral displacement of the southeast corner of the east abutment. 63

Figure 44: Measured lateral displacement of the southwest corner of the west abutment. 63

Figure 45: Measured lateral displacement of northeast corner of east abutment. 64

Figure 46: Measured lateral displacement of northwest corner of west abutment. 64

LIST OF ABBREVIATIONS AND SYMBOLS

α	Angle between width of applied stress distribution from the point of interest
AASHTO	American Association of State and Highway Transportation Officials
AL	Alabama
ALDOT	Alabama Department of Transportation
ASD	Allowable Stress Design
ASTM	American Standards for Testing Materials
β	Angle between the vertical and inside edge of the distributed load
b_q	Width of bearing area
BM	Bench mark
CD	Consolidated Drained
CDOT	Colorado Department of Transportation
CIS	Compaction-induced stresses
CMU	Concrete masonry unit
CRVW3	Three channel vibrating wire data logger
DAQ	Data acquisition system
DL	Dead Load
d_{max}	Maximum aggregate size
DS	Direct shear
EDM	Electronic distance measurement
EOR	Engineer on record

EPC	Earth pressure cell
FHWA	Federal Highway Administration
FS	Factor of Safety
F.S.O.	Full-scale output
ft	Feet
ft ²	Square-feet
GB	Gigabyte
GRS	Geosynthetic Reinforced Soil
H	Height of GRS abutment
HDPE	High-density Polyethylene
IBS	Integrated Bridge System
in	Inches
IM	Dynamic Allowance
k _a	Rankine Active Earth Pressure Coefficient
k _p	Rankine Passive Earth Pressure Coefficient
lbs	Pound force
lbs/in	Pound force per inch
L	Length of bearing area
LL	Live Load
LRFD	Load and Resistance Factor Design
LSDS	Large scale direct shear
MB	Megabyte
MSE	Mechanically stabilized earth

min.	Minute
μ	Friction coefficient
N	Number of traffic lanes
NCHRP	National Cooperative Highway Research Program
No.	Number
ϕ	Angle of Internal Friction
pcf	Pounds per cubic-foot
PET	Polyethylene terephthalate
PI	Plasticity index
PP	Polypropylene
PPT	Pore pressure transducer
PS	Plane strain
psf	Pounds per square-foot
psi	Pounds per square-inch
PT	Performance test
q_b	DL due to the bridge superstructure
Q_{25}	Twenty-five-year flood flow rate
q_{LL}	Total bridge vertical live load
RRFC	Railroad flat car
RSF	Reinforced soil foundation
σ_h	Horizontal earth pressure
SRW	Segmental retaining wall
SSD	Saturated surface dry

S_v	Vertical spacing
T_{allow}	Allowable reinforcement strength
$T_{@ \epsilon=2\%}$	Reinforcement strength at 2-percent strain
T_f	Ultimate reinforcement strength
T_{req}	Required reinforcement strength
TX	Triaxial test
$V_{\text{allow, emp}}$	Allowable vertical stress on the abutment
V_{applied}	Applied vertical stress at surface of abutment
x	Horizontal distance from the point of interest
yd	Yard
yd ³	Cubic yard
z	Depth to the point of interest

CHAPTER 1: INTRODUCTION

1.1 Overview

Geosynthetic reinforced soil-integrated bridge systems (GRS-IBS) consist of closely spaced layers of geosynthetic reinforcement and compacted granular backfill that directly supports the bridge and blends the abutment and roadway for a seamless transition (Adams et al. 2011b). GRS-IBS can be constructed using a small workforce with little impact on the surrounding landscape, and the design can be easily modified to accommodate site conditions (Adams et al. 2011a). GRS construction was first used by the U.S. Forest Service during the 1970s to construct wrapped face walls in the Siskiyou and Olympic National Forests in Oregon and Washington, respectively (Steward and Mohnney 1982).

During the 1980s, the Colorado Department of Transportation (CDOT) modified GRS structures for use as retaining walls along roadways (Wu 1994). GRS-IBS is a modified version of the GRS wall developed by CDOT to account for additional lateral stress (Adams et al. 2011b). GRS-IBS was created by the Federal Highway Administration (FHWA) during the Bridge of the Future Initiative to serve as a lower cost design option for single span bridges in the United States (Adams et al. 2011b). Reports have shown GRS-IBS to be 50 to 60 percent less expensive to construct than traditional bridge foundations (White et al. 2012). In 2010 the FHWA began the Every Day Counts (EDC) Initiative to accelerate the implementation of GRS-IBS within the U.S. Over 200 bridges have been successfully built since 2010 in a variety of environments (Daniyarov et al. 2017).

An example of a GRS abutment constructed using grouted riprap to cover a geosynthetic wrapped face is shown in Figure 1 and Figure 2 shows the west abutment of the Marshall County GRS-IBS as the bridge beams are being placed.



Figure 1: Olympic Avenue GRS abutment in Buchanan County, Iowa. Abutments use grouted riprap over wrapped geosynthetic face for scour protection (photo from Vennapusa et al. 2012).



Figure 2: Placing prestressed concrete box beams onto the beam seat of the Marshall County GRS with segmental retaining wall (SRW) unit facing.

1.2 Objective

The primary objectives of this study are to monitor the construction of Alabama’s first GRS-IBS and to measure the performance of the structure over time. Several tasks were identified to support these objectives, including:

- Recording images before, during, and after construction,
- Measuring pore pressures and earth-pressures within the abutments, and
- Measuring geospatial displacement after construction.

1.3 Scope

The monitoring program for this study used time-lapse cameras, instrumentation, and survey equipment. The time-lapse cameras were installed prior to construction so that each phase of the construction process could be monitored. Pore-pressure and earth-pressure sensors were installed

within both abutments during construction to monitor changes in stress within the backfill. Measurements of geospatial movements were conducted using a total station and survey targets attached to the abutments. To enable a continuous collection of pressure sensor measurements, data loggers were installed and connected to the sensors once the abutments were completed.

This thesis presents background information on GRS-IBS technology and a review of the related literature. The construction of the Marshall County GRS-IBS is discussed, followed by a review of the monitoring program and data collected so far. Conclusions from this study along with recommendations for future research are included.

CHAPTER 2: BACKGROUND AND LITERATURE REVIEW

2.1 Overview of GRS-IBS Technology

GRS-IBS is a component of the FHWA Every Day Counts Initiative and was developed using design concepts from the U.S. Forest Service and later modified by the CDOT (Adams et al. 2011b). The design consists of a compacted granular soil placed within closely spaced layers (usually 12-in. or less) of geosynthetic material (Figure 3). The spacing of the geosynthetic layers is a defining feature of GRS and set it apart from mechanically stabilized earth (MSE) walls which have a similar structure. MSE walls are constructed using either inextensible metal or extensible geotextile strips that are mechanically connected to a proprietary facing element. In reality, a GRS wall is a type of MSE wall constructed exclusively with closely spaced layers of geosynthetic sheets that are wrapped or frictionally connected at the face.

The foundation of a GRS abutment can be constructed of reinforced soil or concrete, depending on the site conditions and the native material being constructed upon. A reinforced soil foundation (RSF) is composed of granular fill material that is compacted and encapsulated with a geotextile fabric. According to Adams et al. (2011b), a RSF provides embedment and increases the bearing width and capacity of the GRS abutment and prevents water from infiltrating underneath the GRS mass from a river or stream crossing. The foundation of a GRS-IBS can be constructed using concrete if the native material is competent bedrock; however, other materials, such as dense sand, may qualify for use of a concrete foundation as well. The RSF should be used in cases where the material is subject to consolidation settlement.

Special design considerations are needed near the top of the abutment. The beam bearing bed receives extra reinforcement to accommodate the extra load from the bridge beams. The area just behind the bridge beams is called the integrated approach. This section is reinforced with equally spaced layers of geosynthetic wrapped around the granular backfill material with a final layer of geosynthetic wrapped around dense-grade base stone. This design helps to alleviate differential settlement between the roadway and abutment.

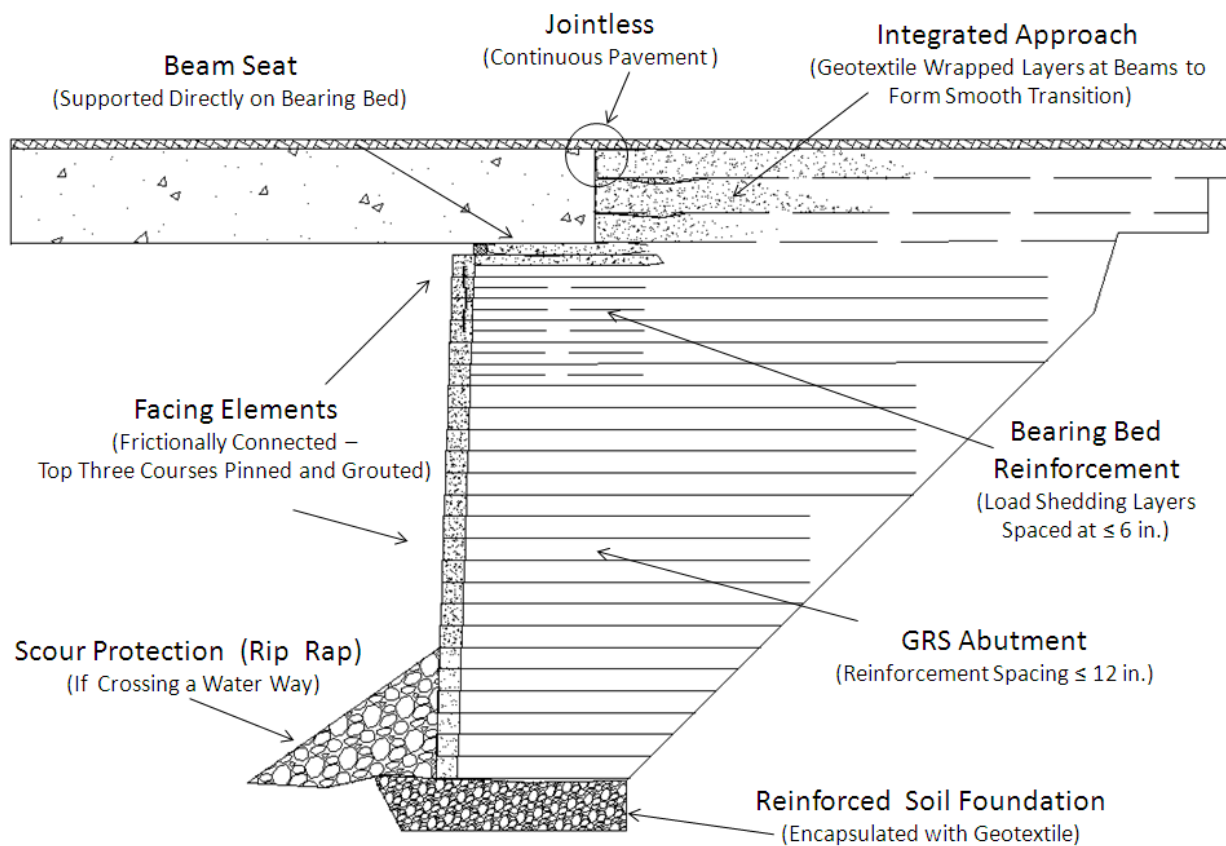


Figure 3: Typical cross section of GRS-IBS (Adams et al. 2011a)

The specific materials used to construct a GRS-IBS will vary depending on the location, site conditions, and the magnitude of stresses that are expected. A variety of facing material can be used based on the desired appearance. The contribution of the facing to the abutment strength is not considered in design, although there is evidence certain facing materials provide additional

capacity (Nicks et al. 2013). The facing material does provide protection against erosion of the GRS backfill due to weathering. The type of geosynthetic used will depend on the material properties of the backfill, reinforcement spacing, and the magnitude of lateral stresses that are expected within the abutment. This is discussed further in Section 2.1.3.

2.1.1 Facing Elements

The primary purposes of the facing element are to provide protection from weathering, serve as a façade, and provide a form for compaction of the backfill material (Adams et al. 2011a). Since geosynthetics carry most of the load in tension, it is often left to the designer to decide on which material will be used for the façade. Modular concrete blocks are commonly used; however, other materials such as wrapped geosynthetics, gabions, full-height concrete, timber, tires, and shotcrete can be used as well (Wu 1994). Wrapped face walls are formed by wrapping extra geosynthetic, used for reinforcement, around the face of the backfill. This requires that the geosynthetic be cut long enough so that it can be covered by the next layer to ensure it is secure. Some GRS walls constructed by the U.S. Forest Service during the 1970s were wrapped face walls and were still in use in 2011 (Adams et al. 2011b). While this is an effective method, damage due to vandalism, fire, and ultraviolet degradation is common (Berg et al. 2009).

Most GRS-IBS structures that have been constructed recently used either segmental retaining wall (SRW) units or concrete masonry units (CMU). Common nominal dimensions of the SRW units and CMU are (10w x 16l x 8h)-in and (8w x 16l x 8h)-in, respectively. A minimum compressive strength of 4000-psi is required, and an absorption limit of 5-percent is recommended in colder climates (Adams et al. 2011a). A freeze/thaw test (ASTM C1262-16) is conducted in these climates to measure the durability and ensure the material meets the standard

specification (ASTM C1372-17). These tests are often independently conducted by a state Department of Transportation.

Large-scale performance tests (PT) conducted by Nicks et al. (2013) showed that facing materials do contribute to the overall performance of a GRS structure, although it is conservative not to include this contribution in design calculations. From their tests, the ultimate bearing capacity significantly increased when CMUs were used as a facing material compared tests conducted without a facing material (Figure 4).

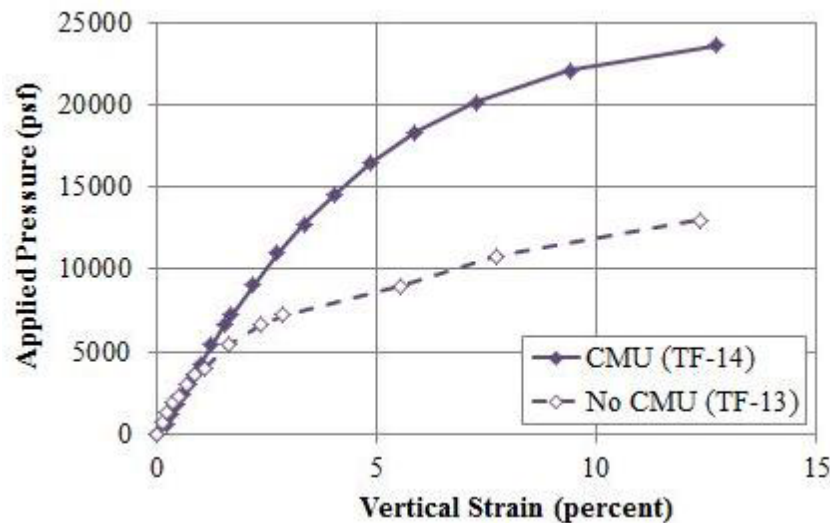


Figure 4: Performance test results of vertical strain with applied load with and without a facing material. The geosynthetic reinforcement was spaced at 11.25-in. with a tensile strength of 3,600 lb/ft (Nicks et al. 2013)

2.1.2 Backfill Material and Scour Protection

The backfill material will affect the performance of the GRS structure, therefore standard specifications for the gradation, strength, and compaction are needed to ensure the quality is adequate. Gradations should be either open-graded or well-graded gravel (Table 1), although lower quality granular or natural fill materials can be used if the quantity of fines is less than 12

percent and a performance test is conducted (Adams et al. 2011a). Furthermore, the material should satisfy American Association of State and Highway Transportation Officials (AASHTO) specifications T 90 and T 104, which limit the plasticity index (PI) and specify measures for the aggregate soundness, respectively. Open-graded backfills are generally used for GRS-IBS since they are not as dense as well-graded gravel, have good drainage, and are relatively easy to compact (Nicks and Adams 2013); however, well-graded aggregates are recommended for use in the RSF and integrated approach so that a denser compaction may be achieved (Adams et al. 2011a). Wu (1994) tested GRS structures constructed with granular and clay materials and determined that many of the soils could be used for the backfill material if they have a low plasticity index and drainage is maintained. Compaction of the backfill material should be 95 percent of the maximum dry density according to the AASHTO T 99 specification. Adams et al. (2011a) recommends using eight-inch lifts compacted with vibratory rollers, and a material with fines should have a moisture content within $\pm 2\%$ of optimum. Open-graded stone can be compacted until no further movement can be visually noticed, but, in all cases, hand operated compaction equipment should be used within 1.5 ft of the face of the abutment and the top 5 ft should be compacted to 100 percent of the maximum density (Adams et al. 2011a).

Table 1: Selected well and open-graded aggregate specifications (after Adams et al. 2011a)

Well-Graded		Open-graded	
Sieve Size	Percent Passing	Sieve Size	Percent Passing
¾ inch	100	½ inch	100
1 inch	94 – 100	3/8 inch	90 – 100
3/8 inch	63 – 72	No. 4	20 – 55
No. 10	32 – 41	No. 8	5 – 30
No. 40	14 – 24	No. 16	0 – 10
No. 200	6 – 12	No. 50	0 – 5

The strength of open-graded aggregates is commonly estimated using an assumed friction angle of 34 degrees leading to overly conservative designs (Nicks and Adams 2013). Direct shear (DS) and triaxial (TX) tests can be used to estimate friction angles; however, these tests require that the maximum aggregate diameter be between 6 and 10 times smaller than the width or diameter of the test specimen, according to ASTM D3080/D3080M and D7181-11, respectively. When using a standard DS device with a specimen diameter of 2.5 in. the maximum aggregate that can be tested is 0.25 in., or in the case of a TX device, with a 2.7 in. specimen diameter, the maximum aggregate size that can be tested is 0.4 in. To overcome this limitation, large-scale direct shear (LSDS) tests have been conducted on open-graded aggregates by the FHWA to estimate a friction angle for design of GRS-IBS abutments. Results presented by Nicks and Adams (2013) indicate a friction angle of 39 degrees is reasonable to use for these materials.

Scour is a concern since the removal of material near a GRS structure has the potential to initiate global failure modes. Interaction between bridge abutments and flowing water can cause erosion at locations near abutments due to the formation of vortex currents (Figure 5). Barkdoll et al. (2007) provides an in-depth discussion of measures that are currently used to mitigate the effects of scour. Recent GRS-IBS designs have included rip-rap and geotextiles as buffers. Other measures to control scour include the placement of sheet piles and grouted rip-rap facings to block the moving water from the GRS and RSF components of the abutment. Combinations of these methods have been used as well. Vennapusa et al. (2012) reported that the use of grouted rip-rap with a rock filled trench at the toe and sheet piles for scour protection had been effective for two projects in Buchanan County, Iowa.

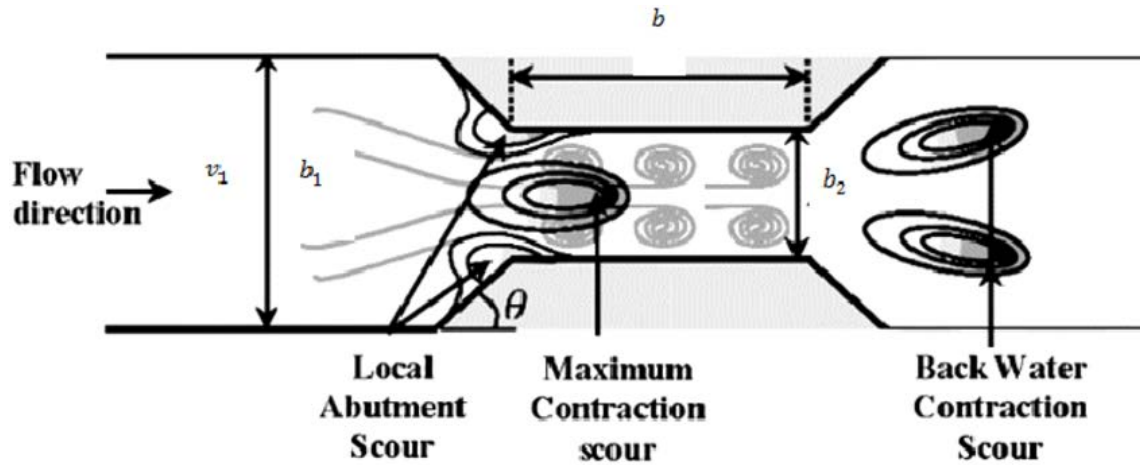


Figure 5: Scour locations near bridge abutments (Ghazvinei et al. 2014)

2.1.3 Geosynthetics

Most GRS-IBS structures have been constructed with polypropylene (PP) biaxially woven geosynthetics (Figure 6); however, other types can be used. Geogrids are polymeric, planar geosynthetics that are formed by intersecting elements known as ribs (Shukla 2002). The method used to connect the ribs can be extrusion, bonding, or interlacing with openings, termed apertures, that range in size from 0.79 to 6 in. and are classified as uniaxial or biaxial (Turnbull 2014) (Figure 7). The apertures provide space for soil to interact with the geogrid, therefore providing additional strength (Figure 8).

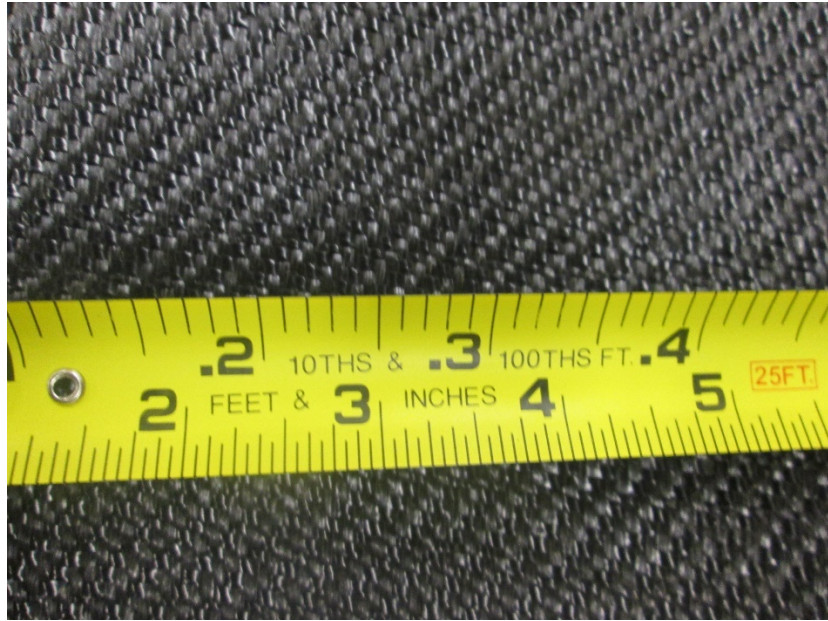


Figure 6: Biaxial woven polypropylene (PP) geosynthetic with rule for scale

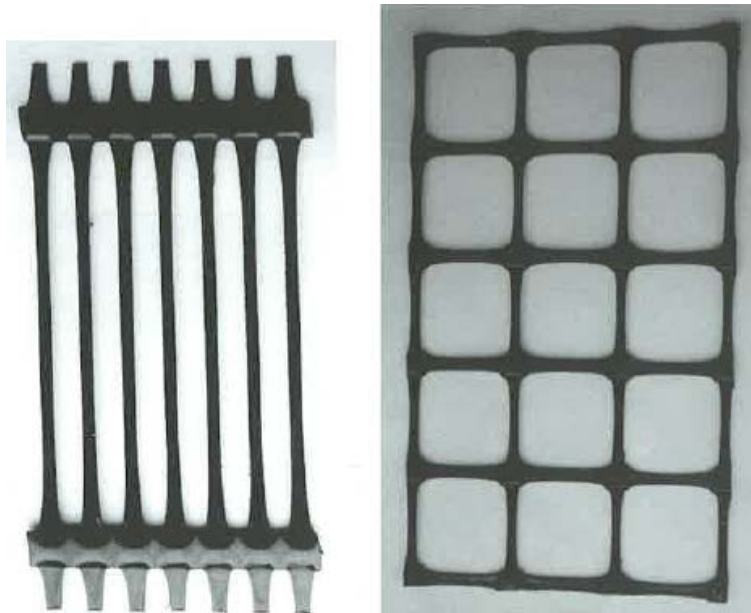


Figure 7: Uniaxial and biaxial geogrids on the left and right respectively (Shukla 2002)

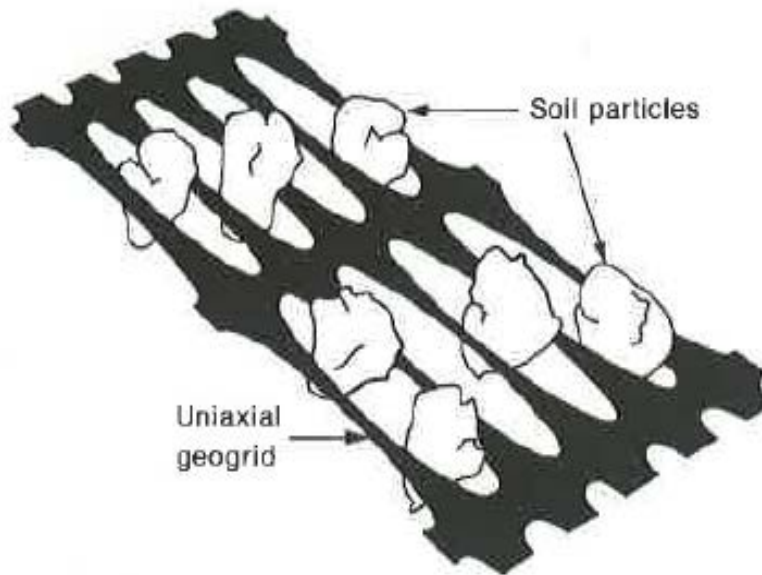


Figure 8: Uniaxial geosynthetic and soil particles interlocked within the aperture space (Shukla 2002)

Soil has good compressive strength but little to no tensile strength; however, geosynthetics perform well in tension (Figure 9), therefore geosynthetics placed in layers, with soil backfill, greatly reduces the lateral stress (Ingold 1994) and allows GRS and MSE walls to be constructed over soft foundations (Holtz et al. 2008). Filtration is also a useful feature of geotextiles that can be used to prevent erosion while allowing pore pressures to dissipate; however, the long-term flow compatibility of the geotextile and soil must be determined using ASTM D5819-18 to reduce the possibility of excessive clogging. When geotextiles are used in combination with the correct soil or aggregate gradation, arches form directly above the geotextile-soil interface creating a bridging network that assists in filtering and mitigates clogging (Koerner 2012).

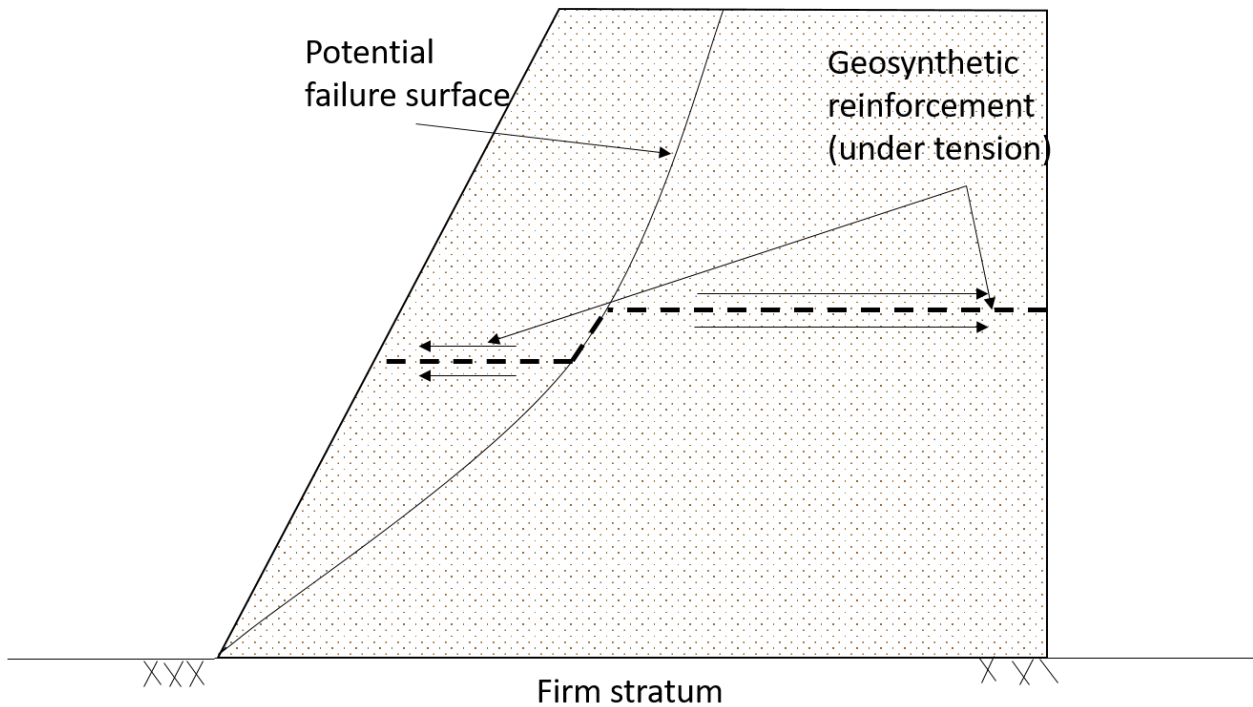


Figure 9: Geosynthetic material placed within soil mass under tension (after Shukla 1992)

Geonets are generally used as a filter on the upper and lower surfaces of geogrid to limit the amount of soil particles that can pass through and interfere with the function of the reinforcement (Turnbull 2014). These materials act as drains and filters to transmit fluid through less permeable soils (Holtz et al. 2008). Transmission of fluid varies among the types of geotextiles, but geonets and geo-composites allow the largest volume of fluid to pass through in applications such as pavement edge, wick, and retaining wall drains (Turnbull 2014).

The type of reinforcement that can be used in GRS-IBS will depend on the lateral stress, spacing of the reinforcement, and backfill properties. The lateral stress imposed on the reinforcement will in turn depend on the dead (DL), and live loads (LL) that are expected during operation. The required reinforcement strength (T_{req}) must be less than the allowable reinforcement strength (T_{allow}) of the geosynthetic and must be less than the strength at 2 percent reinforcement strain ($T_{@e=2\%}$). A minimum ultimate tensile strength (T_f) of 4800 lbs/ft is

recommended for GRS abutments applications (Adams et al. 2011a). Equation 1 provides the relationship of T_{allow} as a function of T_f for a factor of safety (FS) of 3.5.

$$\mathbf{T}_{allow} = \frac{T_f}{FS_{reinf}} = \frac{T_f}{3.5} \quad (1)$$

In situations where flooding is a concern, the geosynthetic must be able to accommodate a fast release of water such that rapid drawdown conditions do not develop within the GRS structure. Drawdown analysis conducted by White et al. (2012) for GRS abutments constructed on 250th Street in Buchanan County, Iowa showed that FS values were slightly lower (1.2 to 1.4) than those recommended by the FHWA (1.5) and recommend using geosynthetics with a permeability of 30-gal/min for GRS-IBS construction.

Uniaxial or biaxial reinforcement can be used for GRS-IBS; uniaxial has greater strength in one direction while biaxial has equal strength in both directions along the length of the roll. Geosynthetics are manufactured as long sheets and packaged in rolls. The “machine direction” refers to the strength along the length of the roll and the “cross machine direction” refers to the strength along the width of the roll (Figure 10). Biaxial reinforcement is recommended for use in GRS-IBS since it reduces the potential for placement errors (Adams et al. 2011a). Standardized testing is used to determine the strength and other material properties of geosynthetics used in GRS-IBS structures (Table 2).

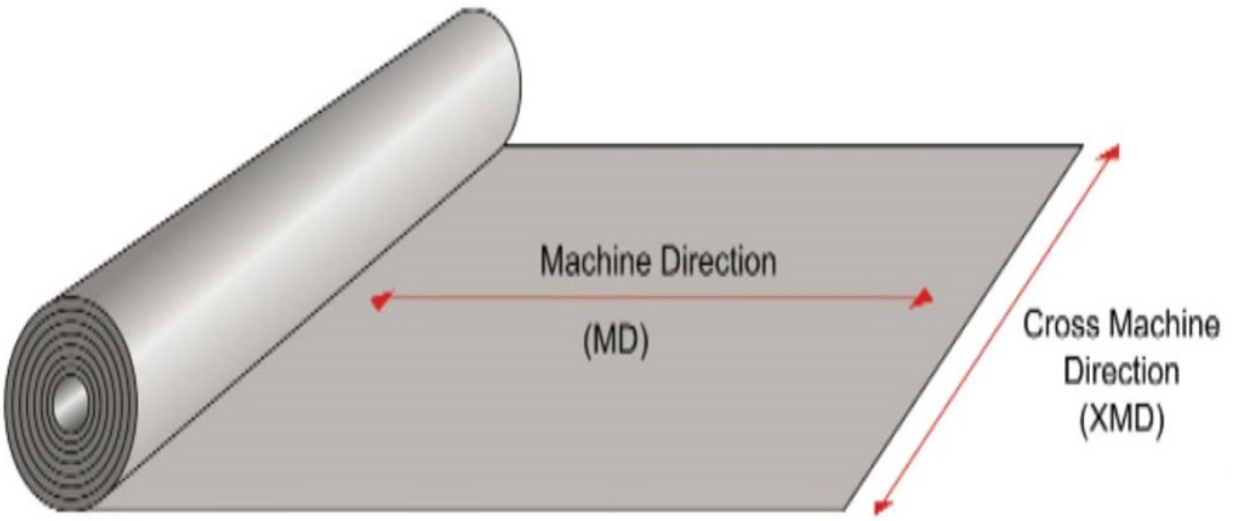


Figure 10: Direction nomenclature for geosynthetic materials (igeosynthetics 2017)

Table 2: Standardized test methods used for geosynthetics in GRS-IBS

Test Procedure	Designation
Wide Width Tensile (geotextiles)	ASTM D4595-17
Wide Width Tensile (geogrids)	ASTM D6637-15
Specific Gravity (HDPE only)	ASTM D1505-18
Melt Flow Index (PP and HDPE)	ASTM D1238-13
Inherent Viscosity (PET only)	ASTM D4603-18
Single Rib Tensile (geogrids)	ASTM D6637-15

2.2 Design Approach

GRS structures have been used for walls, shallow foundations, culverts, and rock fall barriers (Wu et al. 2013), as well as soil improvement (Clyne 2011) and to stabilize slopes (Zornburg 2014). This section will briefly describe the design process for the design of GRS-IBS and its components. The design approach summarized here is primarily based on methods outlined by

Adams et al. (2011a and 2011b) and further information on the design process can be found in this reference. The FHWA design method (Adams et al. 2011a) involves GRS structures that have a vertical or slightly battered wall face and a height that does not exceed 30 ft, usually with a 2:1 base to height ratio or greater. The span of the bridge deck is generally limited to 140 ft, although the bearing stress on the GRS structure should not be allowed to exceed 4000 psf. If the bearing load is expected to exceed 4000 psf, performance tests must be conducted to ensure that the structure is sound with 1 percent lateral strain and 0.5 percent vertical strain used as limit states (Adams et al. 2011a). These strength limits have been shown by other authors to be very conservative. For example, Bathurst et al. (2000), and Hitami and Bathurst (2005) used full-scale and numerical models to analyze the stability of GRS structures and found that they could withstand much higher loads than current designs allow for. Nicks et al. (2013) have also shown that the ultimate bearing strength measured during PTs was 10 times greater than the FHWA limit of 4,000 psf for some cases.

The design of GRS-IBS structures begins with preliminary measurements to determine the geometry of the GRS-IBS structure being considered. Once the dimensions have been established, internal and external modes of failure can be estimated. While the FHWA recommends using load and resistance factor design (LRFD), Adams et al. (2011a) provides an allowable stress design (ASD) and a LRFD design procedure that have been modified to produce similar results. Due to the limited amount of information regarding the internal behavior of GRS structures more research is needed so that LRFD factors can be calibrated for use in GRS-IBS.

When load is applied to the surface of the structure stresses develop within the GRS mass that mobilize the shear strength of the backfill material as well as the tensile strength of the geosynthetic reinforcement. Loads exerted onto the abutments manifest into stress distributions

that act laterally within and on the GRS structure (Figure 11). To estimate the stresses within the abutment, the DLs and LLs are applied to the surface of the approach and abutment as vertical surcharges. The resulting lateral stress distributions from the DLs and LLs, as well as the weight of the GRS backfill and retained soil are calculated using Rankine and Boussinesq stress theories as a function of position and depth.

The active earth pressure is used to estimate the stresses that develop in a GRS structure when load is applied at the surface. In the case of a retaining structure, active earth pressure will mobilize when the backfill mass moves toward the wall face, away from the cut. Since the facing is frictionally connected to the geosynthetic, the wall will move with the backfill. Equation 2 provides the relationship of the active stress coefficient (k_a). This formulation is based on Rankine's derivation and is used in cases where the confining stress has decreased enough to fully mobilize the shear strength of the soil.

$$k_a = \frac{1 - \sin\phi}{1 + \sin\phi} = \tan^2 \left(45^\circ - \frac{\phi}{2} \right) \quad (2)$$

Where ϕ = the internal angle of friction of the soil

The stress distribution on the GRS wall can be calculated using the unit weight of the backfill as shown in Equation 3.

$$\sigma_h = \gamma_s z k_a \quad (3)$$

Where: σ_h = the horizontal pressure for a constant vertical load

γ = the unit weight of the backfill material.

z = the depth to the point of interest.

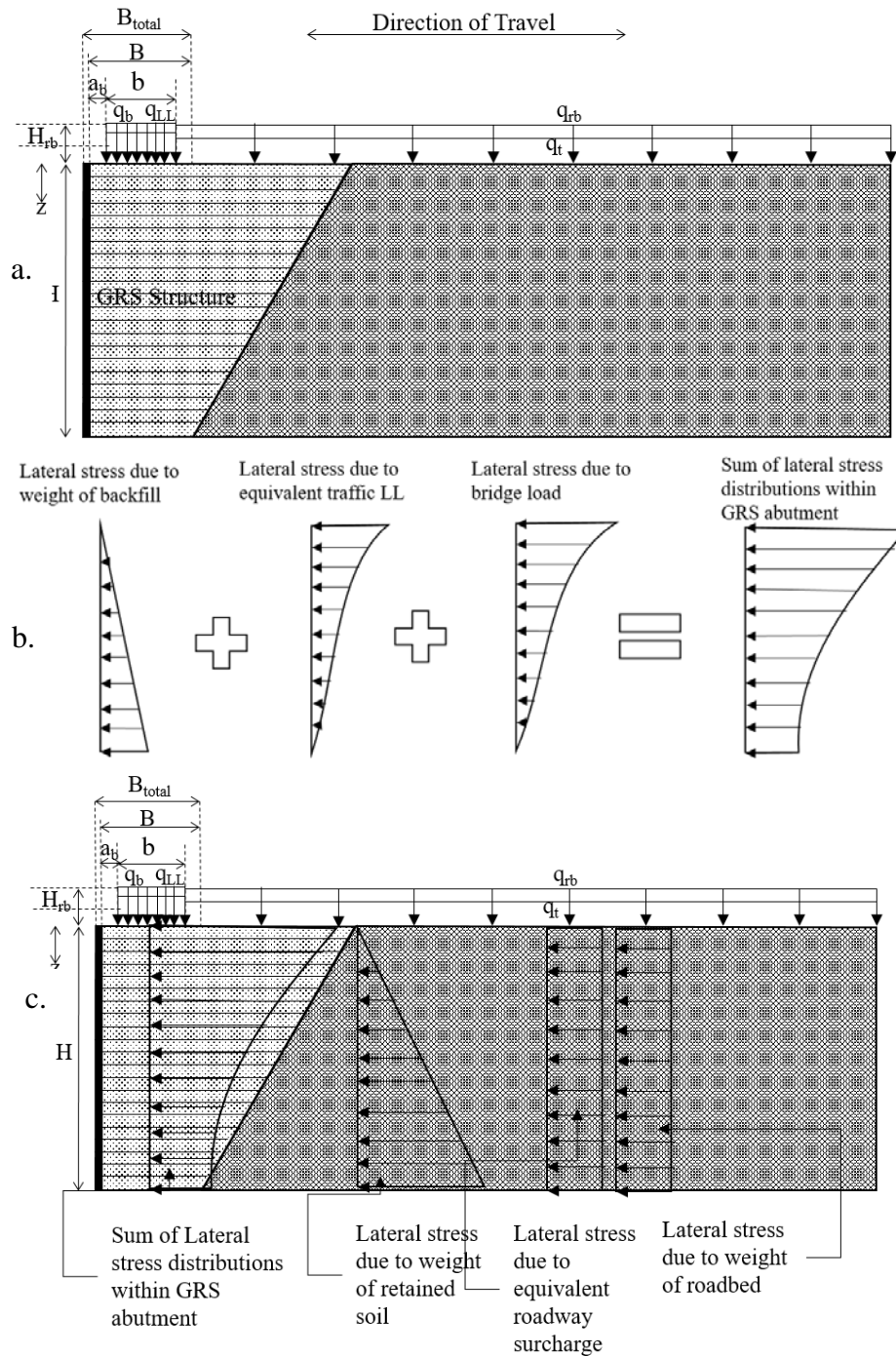


Figure 11: Equivalent stress loads and resultant lateral stresses considered in the design of GRS-IBS: a.) the GRS structure with all DLs and LLs applied at the surface of the abutment and integrated approach, b.) superposition of the lateral stress distributions due to the weight of reinforced backfill, bridge DLs and LLs, and c.) lateral stress distributions due to all vertical loads applied at surface (after Adams et al. 2011a).

The distributions in Figure 11 are estimated using Rankine's lateral stress coefficient, although the true lateral pressures are likely much lower than those calculated using k_a (Allen

and Bathurst 2002, Hatami and Bathurst 2005, Wu et al. 2013, and Wu and Ooi 2015). The effect of surface loads on the lateral stresses can be estimated using Boussinesq stress distribution theory (Figure 12). This formulation is based on small strain, linear elastic theory. Equation 4 shows the formulation recommended by Adams et al. (2011a) for use in GRS-IBS design.

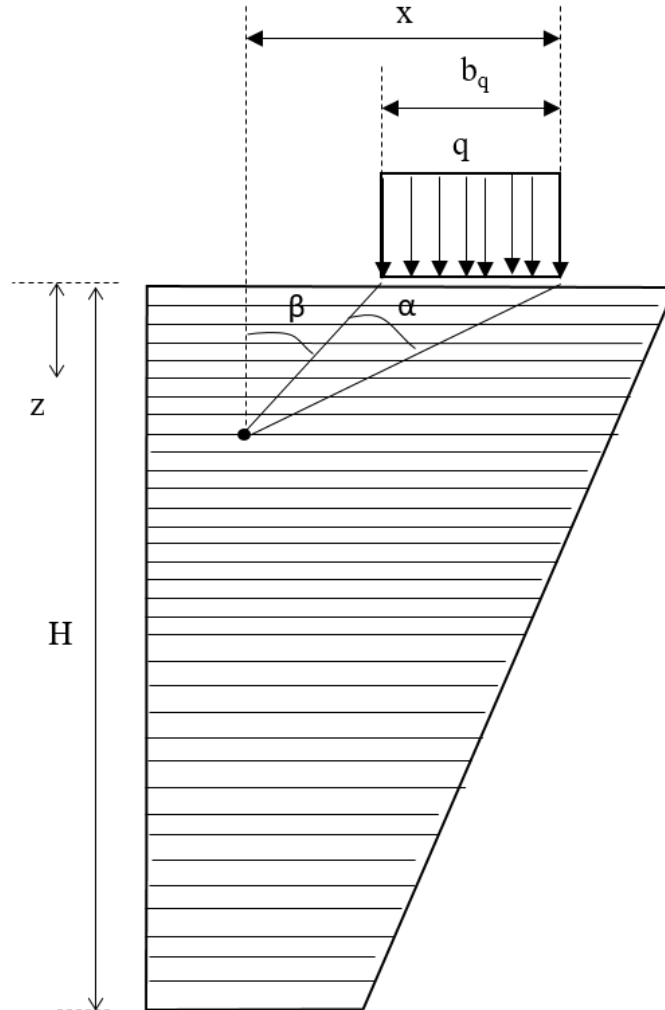


Figure 12: Boussinesq lateral stress in retaining structure due to distributed load at the surface (after from Adams et al. 2011a).

$$\sigma_h = \frac{q}{\pi} [\alpha + \sin(\alpha) \cos(\alpha + 2\beta)] k_a \quad (4)$$

Where: σ_h = lateral pressure at a point,

q = discontinuous pressure across surface of the GRS structure,

α = angle (in radians) between width of the applied stress distribution from the point of interest, and

β = angle (in radians) between the vertical and inside edge of the distributed load at the surface of the GRS structure from the point of interest.

The angles, α and β , are calculated with Equations 5 and 6. In the case of a GRS-IBS structure, the greatest lateral stress will be below the center of the bridge beams.

$$\alpha = \tan^{-1} \left(\frac{x}{z} \right) - \beta \quad (5)$$

$$\beta = \tan^{-1} \left(\frac{x - b_q}{z} \right) \quad (6)$$

Where: x = horizontal distance from the point of interest to the point where the distributed load terminates,

b_q = width of the distributed load, and

z = depth to the point of interest.

The bridge beams, asphalt pavement, and guardrails constitute a distributed DL pressure that induces lateral stresses within the GRS structure and are estimated using the Boussinesq formulation described above. In cases where beams with girders are used, a concrete footing is commonly used to ensure that the load is evenly distributed (Adams et al. 2011a). The approach described above is considered conservative (e.g., Allen and Bathurst 2002, Hatami and Bathurst 2005, and Wu and Ooi 2015) and alternative methods are available. For example, Westergaard theory assumes the soil is reinforced by closely spaced layers which prevent displacement and lower the overall stress development (Naval Facilities Engineering Command 1982), therefore providing a closer estimation of the stresses within a GRS structure.

The LLs on the approach pavement and bridge superstructure must be considered as well. The model for the approach pavement consists of a uniform height of earth that produces an equivalent lateral load in the GRS structure as the application of the specified vehicular LL for the superstructure produces. The uniform height of earth depends on the height of the abutment and is applied perpendicular to the orientation of the abutment with respect to the roadway. Adams et al. (2011a) briefly describes that the contribution of LLs and DLs on the bridge deck are represented by the HL-93 LL model. The dynamic allowance (IM) accounts for the effects of oscillations in the magnitude of the force due to a moving vehicle. Equation 7 shows the relationship given by Adams et al. (2012) to calculate the LL on the superstructure and this concept is further illustrated by Grub et al. (2015). The loading is applied to the bearing area of the GRS abutment (Figure 11) and is simply a way to transfer the effects of the superstructure and traffic to the bearing area of the abutment.

$$q_{LL} = \frac{(LL+IM)*(N)}{\text{bearing area}} \quad (7)$$

Where LL and IM are the live load due to the distributed load and the design vehicle or design tandem and the maximum dynamic loading placed at a position on the bridge to produce the greatest reaction at the abutment. The number of lanes is N and the beam seat bearing area is calculated from the known width of the beam seat and the total width of the bridge. Equation 7 can also be represented as a reaction if the beam seat width is still undetermined at this stage in design.

2.2.1 Global Failure Modes

Three primary global failure modes are considered for design of the GRS: direct sliding, bearing capacity, and global stability. According to Adams et al. (2011a), direct sliding of the

wall is a function of the retained backfill, road base, and the traffic live load surcharge as well as the weight of the GRS structure, bridge and road base. The friction between the base of a GRS structure and the RSF must be estimated using ASTM D5321 or Equation 8. A minimum factor of safety (FS) of 1.5 is adequate for direct sliding.

$$\mu = \frac{2}{3} \phi \quad (8)$$

Where: ϕ = the friction angle of the reinforced granular backfill material

Bearing capacity is calculated based on the vertical pressure exerted by the weight of the GRS structure, bridge bearing seat load, and traffic DL and LL. The equivalent traffic DL and LL account for the super structure as well as the integrated approach. Stress concentrations due to eccentric loading are also considered. A Meyerhof bearing capacity formulation is recommended by Adams et al. (2011a) with a FS of 2.5 or greater.

The potential for global failure is checked using a slope stability analysis to ensure the FS is at least 1.5. This analysis is most often completed using a software program designed for this purpose due to the large number of iterations that are carried out in a limit equilibrium analysis; however, a spreadsheet can be used. It is imperative to gather quality soil property information for this analysis, so estimates will be as accurate as possible, otherwise the critical failure surface may go unnoticed in the analysis.

2.2.2 *Ultimate Capacity*

The maximum pressure allowed on a GRS-IBS is the ultimate bearing capacity divided by a FS equal to 3.5. The maximum bearing capacity is defined as the pressure at 5-percent vertical strain, of the GRS structure, due to the DLs. The allowable empirical stress ($V_{\text{allow, emp}}$) is a

factor of 3.5 less than the ultimate stress as shown in Equation 10. The applied stress, due to the DL and LL of the bridge superstructure must be no greater than $V_{allow, emp}$ (Equation 11).

$$V_{allow, emp} = \frac{q_{ult, emp}}{3.5} \quad (10)$$

Where: q_{ult} = ultimate bearing capacity determined from PT

$$V_{applied} = q_b + q_{LL} \leq V_{allow, emp} \quad (11)$$

Where: q_b = the DL due to the bridge superstructure , and

q_{LL} = the LL due to the traffic on the bridge superstructure.

Adams et al. (2011a) recommends using an empirical relationship of the strain vs bearing capacity, measured during a performance test, to determine the ultimate value (Figure 13). The values in Figure 13 can be used for design if the materials that will be used are similar, otherwise an independent performance or “mini-pier” test should be conducted based on those documented by Adams et al. (2002, 2007) and Nicks et al. (2013); however, an analytical method can also be used (Wu et al. 2013) if the performance test is not feasible.

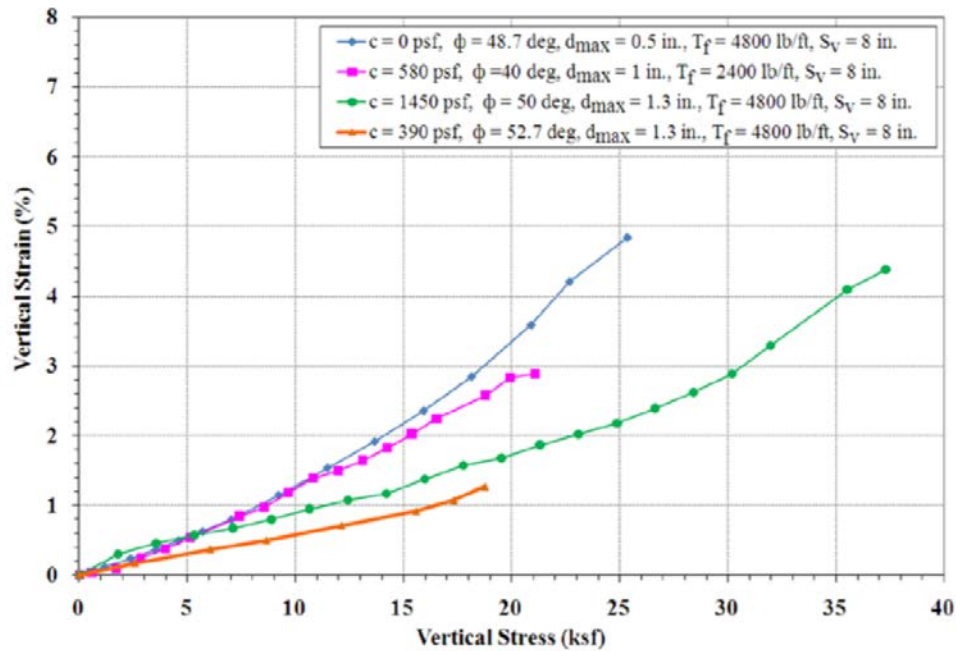


Figure 13: Stress-strain performance design envelopes for vertical capacity, using different compacted reinforced backfills (Adams et al. 2011b).

2.2.3 In-Service Strains

Adams et al. (2011a) recommends that the vertical stress at 0.5-percent strain be used as a limit for the in-service stress of a GRS structure. As with ultimate capacity, Figure 13 can be used to estimate these values or a performance test must be conducted if the materials used are different from those which were used to obtain the curves in Figure 13. Settlement of the in-situ soil should also be considered and estimated using one-dimensional consolidation theory. The lateral strain of a GRS structure is determined analytically by applying the theory of zero volume change and should be limited to 1 percent (Adams et al. 2011a). This assumes that the volume gained will equal the volume lost as the abutment displaces laterally (Adams et al. 2002). Furthermore, the maximum strain depends on the loading and backfill density, but generally occurs within the top third of the GRS structure (Wu et al. 2006, 2013).

2.2.4 Reinforcement Strength and spacing

Wu et al. (2013) provides a formulation to calculate the required reinforcement strength and this relationship is a function of the lateral stress, reinforcement spacing, and the maximum aggregate size (Equation 12). Since the horizontal stress changes with vertical position, strength estimates are needed at each layer of reinforcement. The horizontal stress within the abutment is related to the stress due the backfill material, bridge and roadway DLs and LLs, as previously noted.

$$T_{\text{req}} = \left[\frac{\sigma_h}{0.7 \left(\frac{S_v}{6d_{\text{max}}} \right)} \right] S_v \quad (12)$$

Where: σ_h = the active horizontal earth pressure,

S_v = the reinforcement spacing, and

d_{max} = the maximum aggregate size.

The horizontal stress (σ_h) can be calculated using equations provided by Adams et al. (2011a). Furthermore, Adams et al. (2011a) recommends that the allowable reinforcement strength be at least a factor of 3.5 less than the ultimate tensile strength and less than the strength at 2-percent reinforcement strain. This criterion is extended to the bearing bed as well. The bearing bed reinforcement, spaced at 4 in., will extend to minimum of approximately 3-ft below the base of the beam seat CMU, although the maximum depth and spacing will depend on whether the criteria mentioned above is satisfied. Results from PTs show that reinforcement spacing contributes more to the capacity of a GRS structure than reinforcement strength. Nicks et al. (2013) concluded that PTs with an S_v of less than 12 in. outperformed those with an S_v of 15 ¼ in., while noting that the failure surface for the larger spaced test did not fully mobilize the shear strength of the geosynthetics since soil controlled the failure mode.

2.3 Performance of Selected Bridges

Numerous case studies of GRS have been conducted both before and after the FHWA produced an implementation guide. Some of the structures do not include the integrated approach and use only the geosynthetic reinforcement and granular backfill in their design. Others use all aspects of the design recommended by Adams et al. (2011a). The case studies of the Defiance County, Ohio, Buchanan County, Iowa, and Vermilion Parrish, LA structures are summarized to gain insight into the design, performance, and cost of GRS structures in operation.

Defiance County, Ohio constructed 26 GRS-IBS between 2005 and 2011 at a cost of \$3,513,484 (Bloser et al. 2012). Fifteen of the structures were built by county crews, seven were constructed by a contractor with the assistance of county crews, and the remaining four were built by a contractor. Instrumentation was installed on 5 of the 26, to measure vertical and lateral deformations. Differential settlements of 0.396 in. and average vertical displacement of less than 1.2 in. was observed over a three-year span (Adams et al. 2011a).

The 250th Street GRS-IBS in Buchanan County, Ohio utilized GRS abutments constructed within trenches with sheet pile walls at either end and features railroad flat cars (RRFCs), resting on concrete footings, for the superstructure. Removal of the existing bridge and construction of the GRS abutments was monitored and instrumented using survey targets, earth pressure cells, piezometers, and inclinometers (Vennapusa et al. 2012). The structure consists of three 68.5 ft long RRFCs placed on a concrete foundation that is constructed directly on the GRS backfill. Two sheet pile walls were installed at each end of the abutment (normal to the direction of the roadway) to act as a form for excavation of the native soil and placement of the reinforced backfill. The project was completed in approximately 40 days using county personnel and equipment at a cost of 40 to 50 percent of traditional bridge construction (Vennapusa et al.

2012). Over a period of about a year, maximum settlements of 0.5 in were observed, while transverse differential settlements of 0.2 in were also recorded; however, Vennapusa et al. (2012) also noted most of the settlement occurred within two months after completion of the project.

Recently, the first GRS-IBS in Louisiana was constructed at Maree Michel, on Route LA 91 in the Vermilion Parish (Saghebfar et al. 2017). The GRS-IBS is approximately 14 ft tall with a CMU facing and a 72 ft span steel girder design with a foundation subgrade material that is predominately high plasticity clay (CH) (Saghebfar et al. 2017). Construction of the abutments was completed in about two months, although the integrated approach was finished a few months later due to weather delays. Instrumentation was installed on the south abutment, settlement readings indicated a maximum settlement of about 0.3 in. about 6-months after construction, while a maximum lateral displacement of approximately 0.1 in. was recorded near the top of the structure 2 months after placement of the bridge girders, although measured lateral pressure against the facing was negligible (Saghebfar et al. 2017).

CHAPTER 3: DESIGN OF THE MARSHALL COUNTY GRS-IBS

3.1 Site description

The Marshall County GRS-IBS is located on Cochran Road, which is lightly traveled and connects U.S. Highway 75 to County Road 409 (Figure 14). The bridge spans approximately 40 ft across Turkey Creek. The drainage area for this portion of Turkey Creek is approximately 5 square miles and the 25-year flood elevation of Turkey Creek is estimated to be 8.77 ft above the base of the GRS foundation with a peak runoff rate (Q_{25}) of 1850 ft³/s (ALDOT 2017). Despite this high flow, the potential for scour is low in this area due the hard nature of the bedrock foundation which is exposed in the creek bed. This low scour potential was one of the reasons that this site was selected for the first GRS-IBS in Alabama.

Auburn University researchers visited the site before the project began to visually inspect the existing bridge and site conditions. At this time, no evidence of scour was encountered near or around the existing abutments or the steel I-beam bridge deck supports. During excavation for the GRS-IBS, the channel was widened by approximately 20 ft, which will lower the velocity of the water and help ensure scour will not become an issue during future intense rain events. Even though the site had low potential for scour a portion of the excavated sandstone was placed along the abutment contact and base of the GRS wall to provide additional protection for the new abutments.

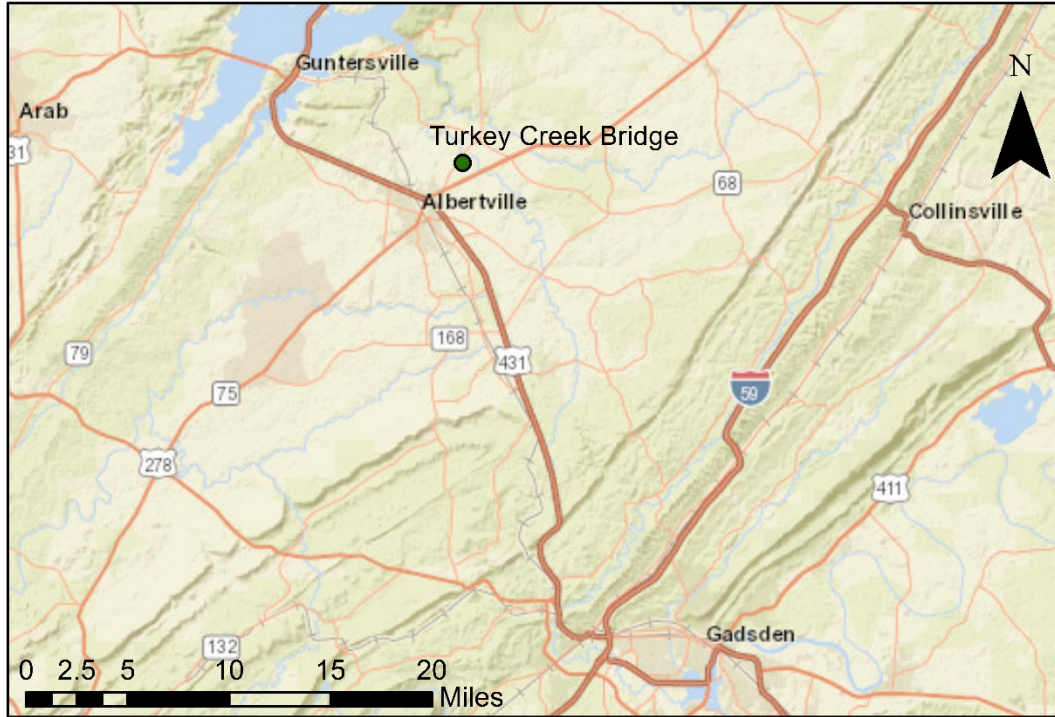


Figure 14: Location of GRS-IBS construction site

3.2 Site Geology

Marshall County is part of the Sand Mountain region of the Cumberland Plateau, the most southerly part of the Appalachian Plateaus province of the Appalachian Highlands Region (Neilson 2007). Sand Mountain is a sub-maturely dissected synclinal plateau of moderate relief capped by the Pottsville Formation (Pomeroy and Thomas 1985). The Pottsville formation derives its name from the anthracite coal field, Pottsville, in eastern Pennsylvania and is separated into four fields based on coal production: The Warrior, Cahaba, Coosa, and Plateau fields (Adams et al. 1926).

These fields were once connected but are separated today due to folding, faulting, and erosion of the highland areas (Adams et al. 1926). The project site is within the Plateau field; however, since the fields were once connected, a cross section of the Cahaba field can be used to identify the general stratigraphy of the area. This consists of interbedded sandstones, siltstones,

claystone, shale, and coal beds, with orthoquartzite conglomerate at the base (Peavy 2008). Rock cores taken at the site (ALDOT 2017) indicate the foundation material is primarily hard sandstone with a 10 to 15-degree dip angle, although thin coal seams were also found. An unconfined compressive strength of 11,300 psi was reported for the sandstone. Borings were completed to a depth of 17 and 14.5 ft on the east and west side of the creek respectively and indicated similar material across the site (Figure 15).

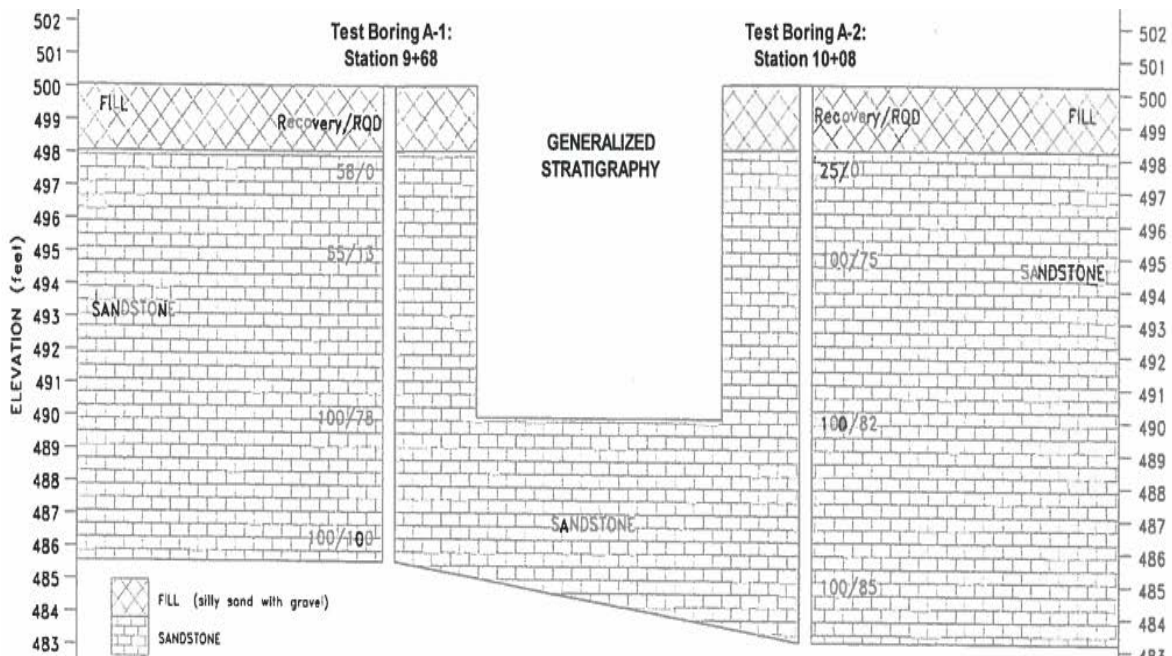


Figure 15: Generalized stratigraphy of GRS-IBS construction site (ALDOT 2017)

3.3 Design

The GRS-IBS at Turkey Creek was designed using the guidance presented in the Federal Highway Administration GRS-IBS Implementation Guide (Adams et al. 2011a) and the GRS-IBS Synthesis Report (Adams et al. 2011b), with some modifications. Initially, three abutment reinforcement configurations were considered and were compared to determine the most efficient design. Constant length, truncated, and stepped reinforcement designs were analyzed to

determine the factors of safety for bearing and sliding as well as the volume of rock excavation that would be required for each design (Table 3).

Table 3: Calculated bearing and sliding factors of safety and volume of rock excavation (after Elton 2014)

Design Type	Constant length	Stepped	Truncated
Bearing FS	5.7	6.0	5.9
Sliding FS	2.9	2.0	1.9
Estimated rock excavation (yd ³ /yd)	12.78	9.04	8.63

Each design provided the required capacity for bearing and sliding failure, so the truncated method was selected to reduce the quantity of material that needed to be excavated. The overall dimensions of the abutments are approximately 12 ft high and 33 ft wide, while the wingwalls are approximately 6 ft wide at the base, transitioning to a maximum of 10 ft wide at the road surface (Figure 16). A 6 in. thick concrete foundation was constructed on the native sandstone using ready-mixed concrete to serve as a leveling pad for the wall.

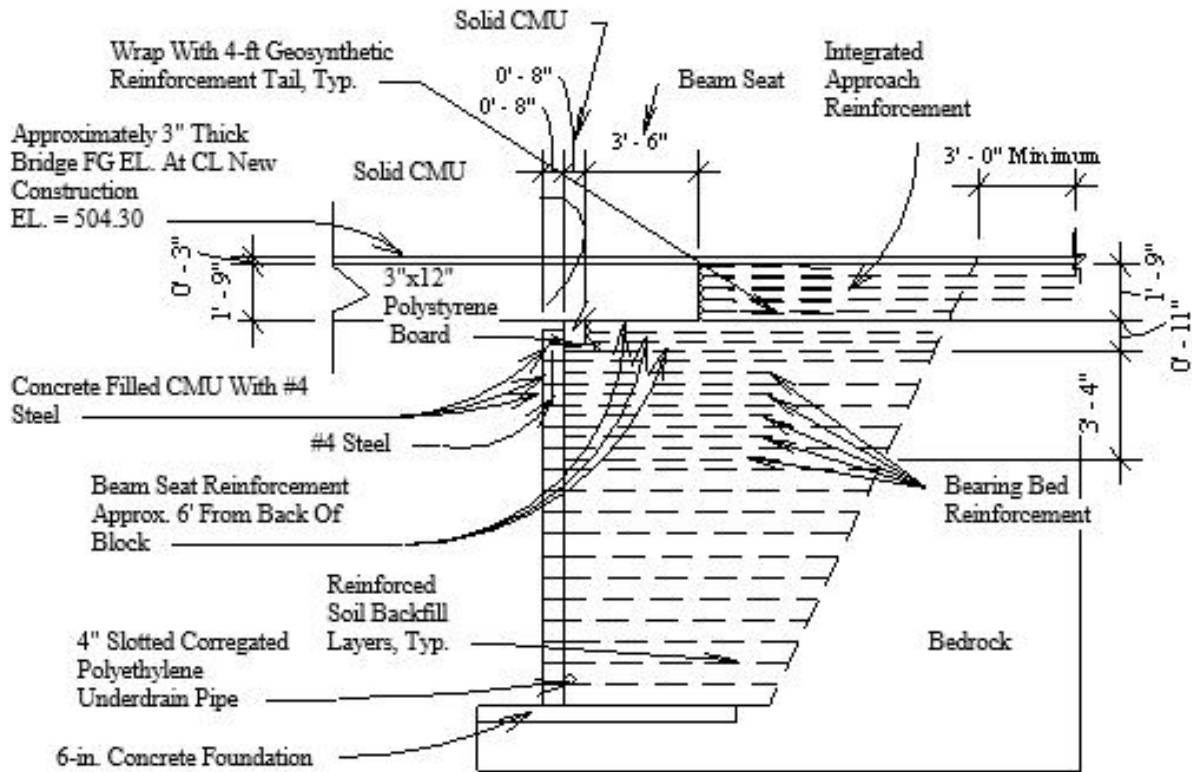


Figure 16. Design profile of GRS-IBS in Albertville, AL (after from ALDOT 2017).

The reinforced backfill was constructed using No. 89 limestone gravel and biaxial woven geosynthetic spaced every 8 in. and extending to the cut-slope. Additional reinforcement was placed in the bearing bed and beam seat areas to accommodate the extra load of the bridge deck (Figure 16). At the surface, the integrated approach consists of 3 layers of reinforcement that extended at least 3 ft beyond the surface projection of the cut-slope to reduce differential settlement.

3.4 Materials

The GRS abutments were constructed using U.S Fabrics Type 4800 woven geosynthetic (Figure 17a) and No. 89 limestone gravel. The specified gradation for the gravel is shown in Table 4. Auburn researchers performed Standard Proctor density tests on the No. 89 stone which indicated the as-placed dry unit weight was approximately 105 pcf. This geosynthetic material

was tested independently, by SGI Testing Services, using the ASTM D 4595 wide-width tensile strength test (Table 5). The GRS abutments were faced using segmental retaining wall (SRW) cement masonry units (Figure 17b). Some of the measured properties for the SRW masonry units are listed in Table 6. The SRW blocks were selected as they had low absorption, which was considered important to the long-term performance of the facing. The bridge deck was constructed using seven 52 ft long by 4 ft wide by 1.75 ft thick prestressed concrete beams. This consisted of five middle beams and two end beams with cross-sectional areas and calculated weights of 4.7 ft² and 5.6 ft² and 36,956 lbs and 43,651 lbs, respectively.



Figure 17. (a) Selected woven geosynthetic; (b) segmental retaining wall masonry units.

Table 4. No. 89 stone gradation results (after from ALDOT 2017)

Sieve Opening	Test 1	Specification
½ in. (12.5 mm)	100.0	100
3/8 in. (9.5 mm)	97.0	90-100
#4 (4.75 mm)	33.0	20-55
#8 (2.36 mm)	9.0	5-30
#16 (1.18 mm)	4.0	0-10
#50 (300 µm)	2.0	0-5

Table 5. Selected tensile strength measurements of the 4800 geosynthetic (after from SGI Testing Services, LLC 2017)

Test No.	Tension at 2% lbs/in	Tension at 5% lbs/in	Tension at 10% lbs/in	Ultimate Strength lbs/in	Ultimate Strain (%)
1	38	146	302	465	18.2
2	45	155	311	446	17.6
3	46	158	310	465	19.2
4	38	147	302	449	17.8
5	37	144	294	454	19.8
6	37	148	309	455	17.6
Mean	40	150	305	456	18.4

Table 6. Selected test results (ASTM C140-16 and ASTM C1372-16) of segmental retaining wall masonry units (after S&ME 2017)

Unit No.	1	2	3	Average
Received Weight, lbs	94.31	93.85	93.34	98.83
Width, in.	10.9	11.0	10.9	10.9
Height, in.	8.0	8.0	8.0	8.0
Front length, in.	18.0	18.0	18.0	18.0
Back length, in.	11.0	11.0	11.0	11.0
Compressive strength, psi	10,220	8,640	8,610	9,160
Saturated (SSD) wt., lbs	56.27	55.25	54.66	55.39
Oven Dry wt., lbs	54.66	53.79	53.20	53.88
Absorption, %	2.9	2.7	2.7	2.8
Density, pcf	144.0	143.6	144	143.9

Furthermore, three consolidated drained triaxial tests were also conducted on the No. 89 stone by Auburn researchers to estimate the strength of the material. Confining stresses of 7.5, 12.5, and 17 psi were used, and the friction angle of the material was estimated to be 46 degrees (Figure 18). The secant shear modulus was estimated to be approximately 10,129 psi using about

0.6-percent strain as the limit of the linear range on the stress-strain plots from the CD tests (Figure 19). As the material dilated during shearing, strain hardening became prominent as well.

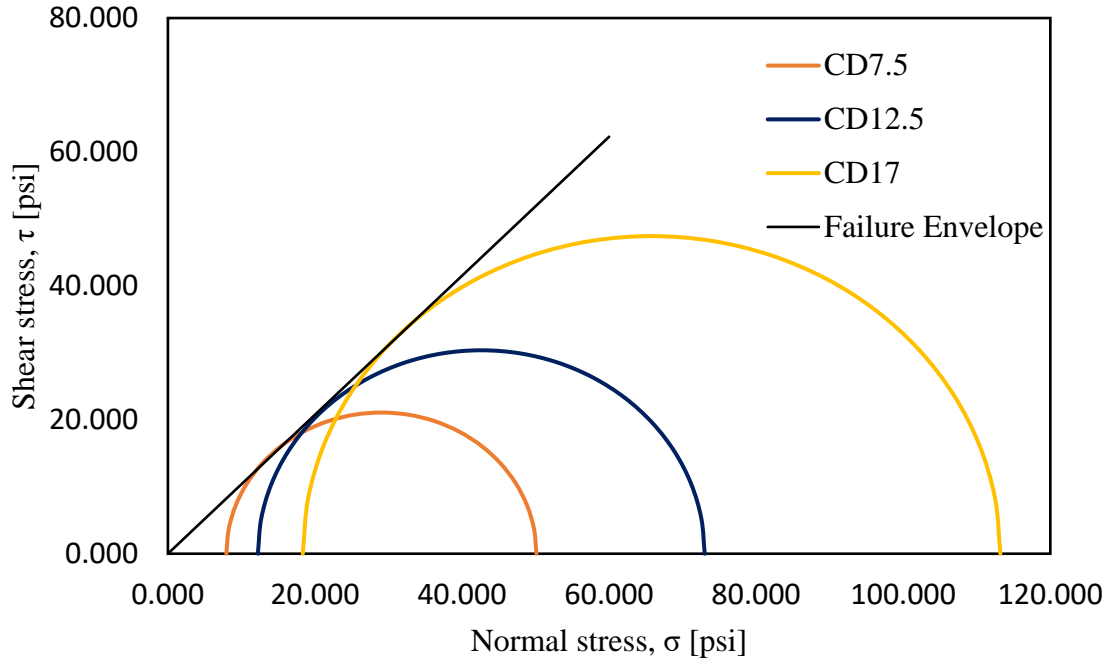


Figure 18: Mohr-Coulomb failure criteria for No. 89 backfill.

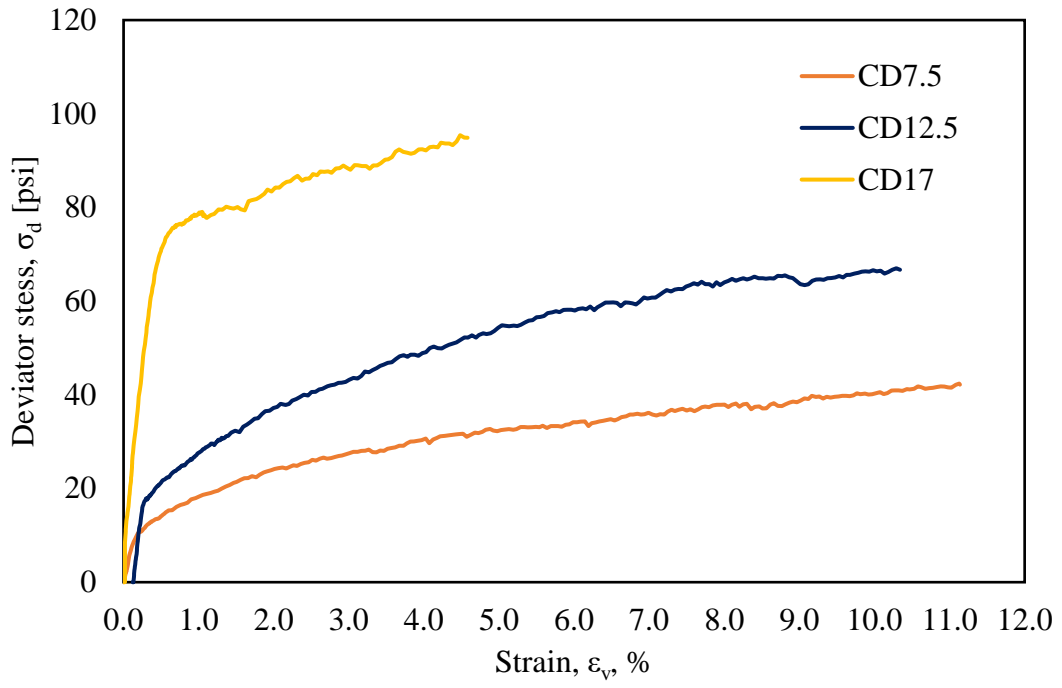


Figure 19: Stress-strain behavior for No. 89 backfill material.

CHAPTER 4 CONSTRUCTION PROCESS

4.1 Demolition and Excavation

Construction of the Marshall County GRS-IBS bridge began on October 2nd, 2017 with the removal of the existing bridge and excavation of the native material (Figure 20a). A hydraulic excavator was used to remove the existing bridge and abutments, and the surficial soil and rock. As the foundation material is primarily hard sandstone, blasting was needed to excavate the abutment down to the required elevation. The excavator was used to remove the blasted material (Figure 20b). Berms constructed from the native material were used to limit the inflow of water from the creek into the excavation, but this was only mildly effective, and pumps were used to dewater the excavation prior to placement of the concrete pad.



Figure 20: (a) Removal of the existing bridge at Turkey Creek; (b) removal of blasted sandstone, on the western side of Turkey Creek.

4.2 Concrete Foundation

A concrete leveling pad was placed in each abutment after completion of the excavation. The leveling pad was 6 in thick, 8 ft deep and 33 ft wide. The concrete forms were set at the correct elevation, 490.33 ft, using a traditional tripod mounted level and grade-rod (Figure 21a). Ready-mixed concrete was brought to the site and placed using a concrete bucket attached to a hydraulic excavator (Figure 21b). Concrete was initially placed around the outside of the form boards to keep concrete from leaking out of the formwork. Once the concrete placed around the perimeter hardened, concrete was placed within the formwork and finished using traditional hand tools. Surface grinding was performed on the finished pad as needed to obtain a level surface for block placement.

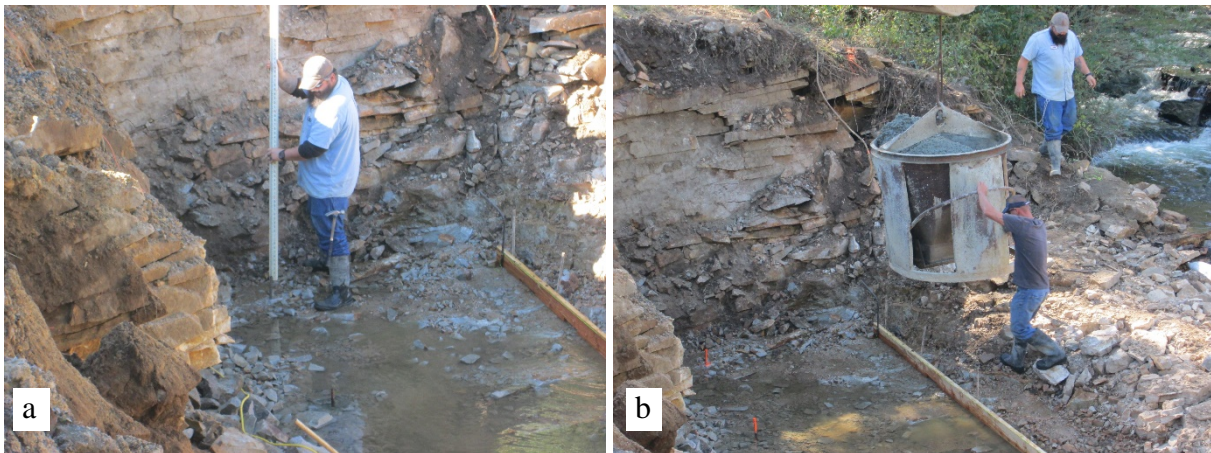


Figure 21: (a) Leveling form boards in the excavation for placement of the concrete pad; (b) Concrete being placed using a concrete bucket suspended from a hydraulic excavator.

4.3 GRS Abutment

The initial row of masonry blocks for the GRS abutment was placed on the concrete foundation by hand using a string-line as a guide and the centers of the blocks were filled with concrete. The area behind the blocks was filled with No. 89 backfill material, which was leveled and lightly compacted to be even with the top of the first row of blocks (Figure 22a). The first layer of geosynthetic material was placed at this elevation (Figure 22b) then the second row of

masonry blocks were set into place. Joints between the blocks were offset with the row of blocks below. A 4 in. corrugated drain pipe was placed behind the second course of blocks to allow for drainage of the backfill. The process of backfilling the masonry blocks with No. 89 backfill material and adding a layer of geosynthetic every 8 in. was repeated for a total of 17 layers at a batter of 1:32. The final three rows of masonry blocks were reinforced and grouted using No. 4 rebar bars placed on 8-in. centers and ready-mixed concrete, respectively.

The area of the abutment directly below the bridge beam seat received extra reinforcement to carry the extra load of the bridge deck. Beginning at elevation 498.33 ft and ending at the top of the abutment, the spacing of the geosynthetic for the bearing bed is 4 in. and extends 6.5 ft from the back of the masonry blocks. An 11 in. wide beam seat was constructed immediately below the beam elevation using closely spaced geosynthetic and No. 89 backfill material that extends 6 ft from the back of SRWs. The final GRS wall is shown in Figure 23.



Figure 22: (a) Placement of initial layer of No. 89 stone to top of first row of masonry blocks and (b) placement of geosynthetic and second row of masonry blocks.



Figure 23: The finished GRS abutment prior to placement of the bridge beams.

4.4 Beam Placement

Precast bridge beams were placed on December 8th, 2017, approximately 54 days after placement of the final concrete bearing pad. The bridge beams are directly supported by a solid concrete masonry unit (CMU) placed on a 3 x 12 in. polystyrene board at the top of the reinforcing layer of the abutments, therefore leaving a 3 in. space between the abutment and bottom of the beams (Figure 24). The beams were placed using a crane and then post-tensioned using three 1 in. diameter steel tie-rods.

The integrated approach, placed after the beams were set, starts just behind the beams and extends a minimum of 3 ft from the end of the beam. The approach consists of four, closely spaced, layers of geosynthetic folded around No. 89 backfill material and a final layer of geosynthetic folded around dense-grade base stone ending level with the top of the bridge beams. The completed approach is shown in Figure 25.



Figure 24: Bridge beam setting on top of CMU with 3 in. gap between abutment and beam and integrated approach reinforcement layer. The circular opening for post-tensioning can be seen at the end of the beam.



Figure 25: Placed bridge beams and the integrated approach.

4.5 Final Grading and Paving

Rain and utility conflicts delayed final grading and paving for approximately two months after completion of the integrated approach. These operations were completed on May 22nd, 2018. Once paving was complete, guardrails were installed, and the bridge was opened for traffic on June 3, 2018. The finished road and bridge is shown in Figure 26. The entire construction process took approximately nine months from demolition of the existing bridge to opening of the bridge.



Figure 26: The completed GRS-IBS over Turkey Creek in Marshall County, AL.

4.6 Construction Issues

Construction of the abutments proceeded as expected for the most part. Minor problems with the initial placement of the foundation and poor dimensional tolerances of the SRW units caused issues. The engineer of record (EOR) prevented a mishap by checking the span length relative to

the layout of the initial row of SRW units. Evidently, the contractor had begun placing the initial row of SRW units such that the final span length would have been greater than the design length of 40 ft. This would have reduced the bearing area, thus increasing the pressure on each abutment. Fortunately, the EOR made sure the issue was corrected before the project was allowed to move forward. Furthermore, as the wall was constructed, the contractor had to trim the corner SRW units to match the row units. While this was an easy solution, it was imperative to ensure that each layer is level, otherwise gaps and loss of the frictional connection would occur. The gaps could provide access for backfill material to migrate out, therefore reducing the structural integrity and the loss of a frictional connection may allow the facing to become unstable.

CHAPTER 5: INSTRUMENTATION

The Alabama Department of Transportation (ALDOT) chose the Turkey Creek site to be a demonstration project for the use of GRS-IBS technology in Alabama. As this is the first bridge of this type to be constructed in the state, ALDOT requested that the construction process and subsequent performance of the bridge be monitored and documented. Auburn researchers worked with ALDOT and Marshall County engineers to design an instrumentation and surveying program to meet this need. The instrumentation consisted of earth and pore pressure sensors, along with time-lapse cameras and periodic surveys to monitor the performance of the bridge.

5.1 Time-lapse Cameras

Two Wingscapes time-lapse cameras with a resolution of 8.0-megapixels were used for this project (Figure 27). The cameras were set to 15- and 30-min. time intervals and placed to obtain the best view possible before, during, and after construction. Sixteen gigabyte data cards were used to store images, which were downloaded periodically.



Figure 27: Wingscapes time-lapse camera used for the project, right photo shows the programming panel on the inside of the cover (Wingscapes 2015)

5.2 Piezometers

Two 4500 Geokon standard vibrating wire piezometers were used for the project (Figure 28). These sensors have a thin wire located within a stainless-steel housing that transmits a frequency based on the tension of the wire (Figure 29). The wire is connected to a diaphragm at one end that deflects in or out based on the applied pressure. Once connected to a DAQ or handheld testing device, an excitation voltage is transmitted thereby causing the wire to vibrate so the resulting frequency can be measured. Since the frequency is dependent on the tension in the wire, the pressure can be calculated using calibration constants determined from factory or independent testing. The typical accuracy and resolution of a vibrating wire sensors is equal to

0.01 and 0.025 percent of the full-scale output (F.S.O.) which is obtained by recording the output frequency at the maximum rated pressure of the sensor (Geokon 2017). For these sensors to produce accurate results they must be fully saturated; however, they can operate in partially saturated clays, although if there is difference in the pore water and air pressures, the sensor will measure the air pressure.



Figure 28: Model 4500 standard vibrating wire piezometer (Geokon 2017)

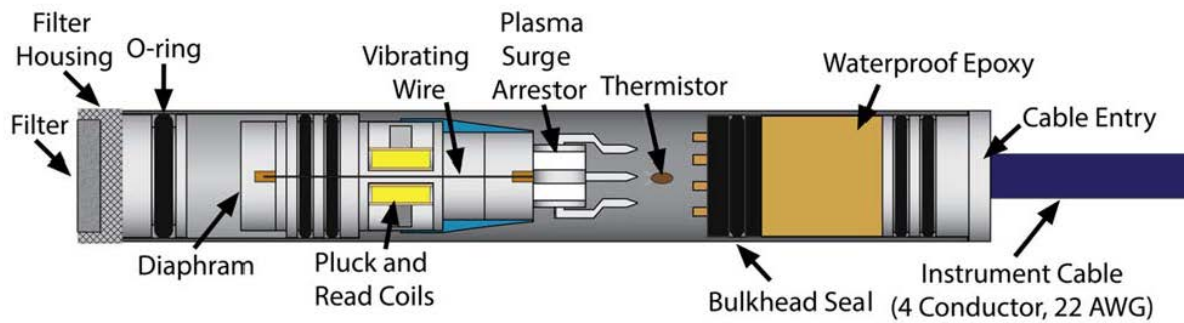


Figure 29: Internal components of vibrating wire sensor (Geokon 2017)

The piezometers are located at an elevation of 491.00-ft, at the approximate center of the abutments near the location of the earth pressure cells (Figure 30). The piezometers were saturated before installation using water from the nearby creek. Then the sensors were inserted into sand-filled sleeves, so they would not be damaged by the backfill material. The cables were routed along the length of the abutment and through a small opening in the SRW units created with a chisel and hammer (Figure 31). Once the wires were in-place, baseline readings were recorded, and the excess wire was stored in 5-gallon containers until the GRS structure was completed.

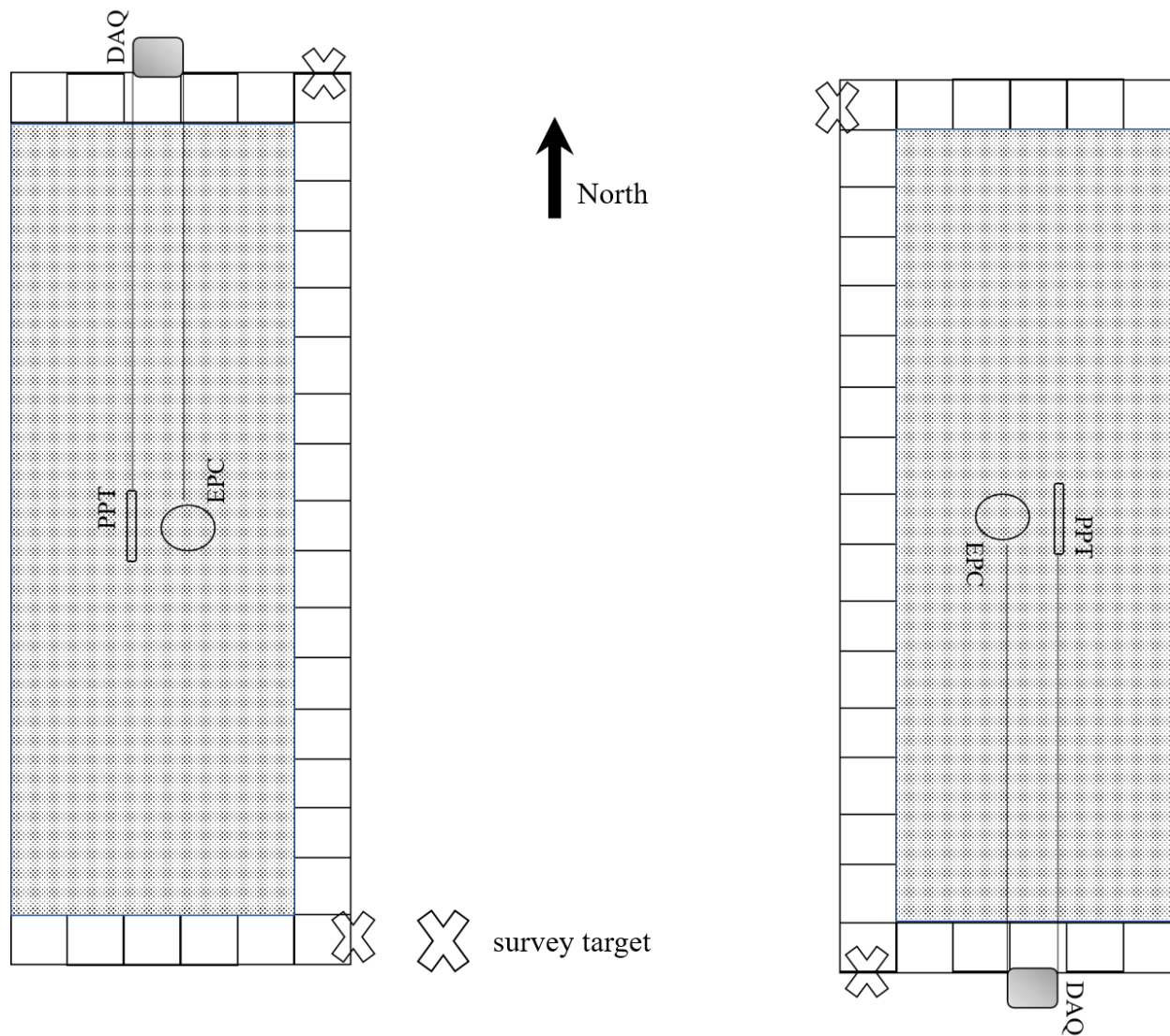


Figure 30: Plan view of the layout of the sensors and survey targets used on the GRS-IBS structure.



Figure 31: Sensor cables routed through chiseled openings in the SRW units.

5.3 Earth-Pressure Cells

Model 4810 vibrating wire earth pressure sensors were used for the project (Figure 32). These sensors are designed to be mounted within a concrete structure or onto an existing structure, such as a concrete foundation and operate by measuring the frequency generated by a vibrating wire that is activated by an excitation voltage (Figure 29). The tension force on the wire is proportional to the pressure exerted onto the instrument from the weight of the overburden. Once pressure is exerted onto the circular plate, oil contained within the instrument causes the diaphragm to deflect, thereby changing the tension of the wire. This instrument measures total stress, therefore pore pressure sensors are needed so the effective stress can be estimated.

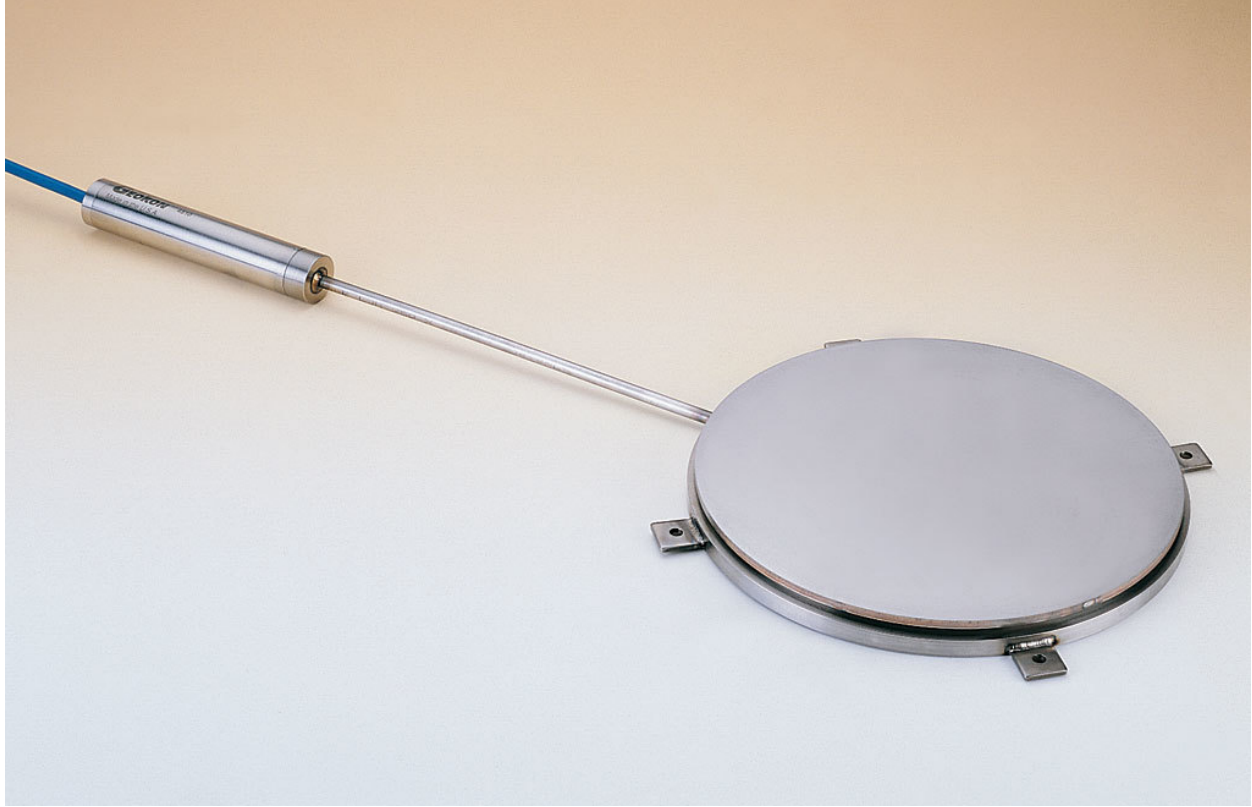


Figure 32: Model 4810 contact pressure cell (Geokon 2017)

Each EPC was installed approximately 3 ft from the face of the SRW units and at elevations of 491.00 and 490.33 ft, for the east and west abutments respectively. This corresponds to 8 in. above the concrete foundation of the east abutment and directly on the concrete foundation of west abutment. During installation, finely-graded sand was used to cover the sensors (Figure 33) to reduce the effects of soil arching.



Figure 33: Installed earth and pore pressure sensors covered with sand to mitigate arching

5.4 Data Loggers

In order to measure the output signal as well as supply excitation voltage, two Campbell Scientific CRVW3 data loggers were used (Figure 34). These DAQs are specifically designed to be compatible with vibrating-wire sensors and have 16 MB of storage. The units were preprogrammed to perform data reduction by adding the sensor conversion constants prior to installation. The unit uses a Fast-Fourier Transform to identify the prominent frequency in the output signal at each time interval.



Figure 34: CRVW-3 data logger used for project (Campbell Scientific 2018)

Once the final course of blocks had been placed, the data loggers were mounted on the southeast and northwest sides of the east and west abutment using concrete screws and construction adhesive. The uneven face of the SRW units made it difficult to fasten the loggers to the abutments with the concrete screws, so construction adhesive was used to help to create a secure fit. Once secured, the instrumentation cables were encased in conduit and mounted to the SRW units and routed into the data loggers. Each sensor has five wires (a thermistor, ground, excitation, and two signal receiving wires) that were connected to the data loggers. After wiring was completed, each DAQ was connected to a laptop computer to ensure that readings were being recorded. Readings have been collected continuously since February 2, 2018 and the data are downloaded approximately every two weeks.

5.5 Survey Instrument and Targets

A Topcon GTS-235W was used to measure geospatial data for the project (Figure 35). This instrument has a laser plumb and vertical and horizontal angle tilt correction sensor that ensures accurate readings. The survey targets used for the project were Berntsen RS60 (Figure 36). These targets are reflective and compatible with a total station. The size of the reflective cross section is 1.57 x 1.57in., therefore the approximate recommended minimum and maximum range is 33 and 328 ft, although according to Berntsen (2018) most total stations can exceed the maximum value.



Figure 35: Topcon GTS-235W total station



Figure 36: RS60 survey target mounted onto a GRS abutment.

Four survey targets were placed at each corner of the abutments using construction adhesive. A fifth survey target was placed on a power pole just east of the project, to use as a bench mark (BM) for subsequent surveys. The BM target was mounted about a foot from the surface of the ground onto the power pole using wood decking screws. Regular surveys were conducted to monitor the movements of the abutments. Surveys began after the bridge beams were placed, on February 9, 2018 and have been conducted approximately every two weeks since then.

CHAPTER 6: RESULTS AND DISCUSSION

The pore-pressure and earth-pressure sensors were monitored periodically during construction of the bridge and have been read on a continuous basis in the following months using data loggers. Surveys began after the bridge beams were placed, on December 7, 2017, and have continued to be conducted approximately every two weeks since.

6.1 Earth-Pressure Measurements

Readings from the earth pressure sensors in the east and west abutments are shown in Figure 37. The earth pressure sensors were manually read, immediately after placement, to establish a zero reading. Manual readings were also taken after completion of the abutment, but prior to placement of the bridge beams. The reading at this time was approximately 600 psf. This is approximately half of the vertical stress that would be expected based one-dimensional stress conditions using the height of the backfill and the estimated unit weight. This value is consistent with the patterns observed experimentally and numerically by Bathurst et al. (2000) and Hatami and Bathurst (2005). They attributed this lower vertical stress to load shedding due to friction of the GRS material on the inner face of the (CMU) (Hatami and Bathurst 2005).

After placement of the bridge beams the stresses in both abutments increased significantly and stresses have continued to increase since then although at a smaller rate. The latest stress readings for both abutments are approximately 1800 psf. The weight of the prestressed concrete bridge beams and backfill material is estimated to apply 1200 psf to the surface of the abutment.

This would suggest the weight of the abutment is contributing approximately 600 psf, which is consistent with the reading taken prior to placement of the bridge beams.

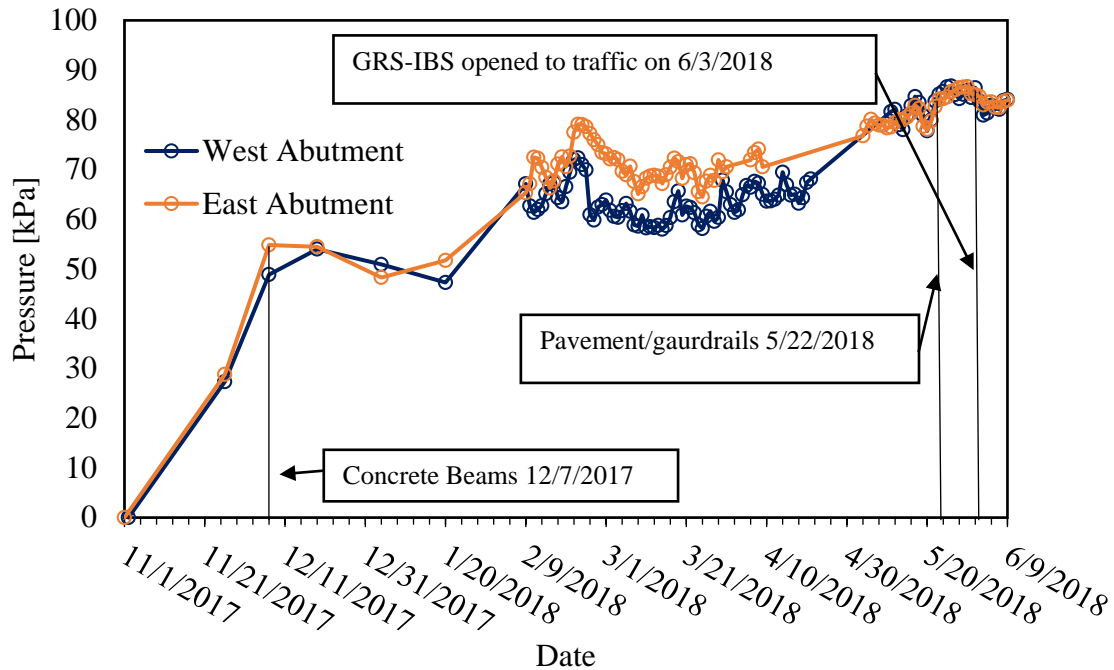


Figure 37: Earth pressure sensor readings show the increase in earth pressure as load is applied in the east and west abutments

6.2 Pore-Pressure Readings

The pore-pressure sensors have shown little to no pore-pressure, as expected (Figure 38). The abutments appear to be dry and the creek has not remained high enough to saturate the lower backfill. Due to this lack of saturation, the specific pressure values shown in Figure 38 may not be accurate. The piezometers are not designed to read pressure in unsaturated sand or gravel and have a range of 7200 psf. While the pressure readings are well within the resolution of the piezometers, the lack of full saturation most likely distorts the readings.

Possible sources of the oscillations in the data include electrical noise created during excitation of the sensor wire as well as movement of the wire itself and external noise emitting from the electrical power transmission lines which run along the side of the bridge. The air entry

value for the No. 89 backfill material is lower than that of the porous stone on the sensor, therefore changes in air pressure will also have an impact on the readings as the sensors are no longer saturated.

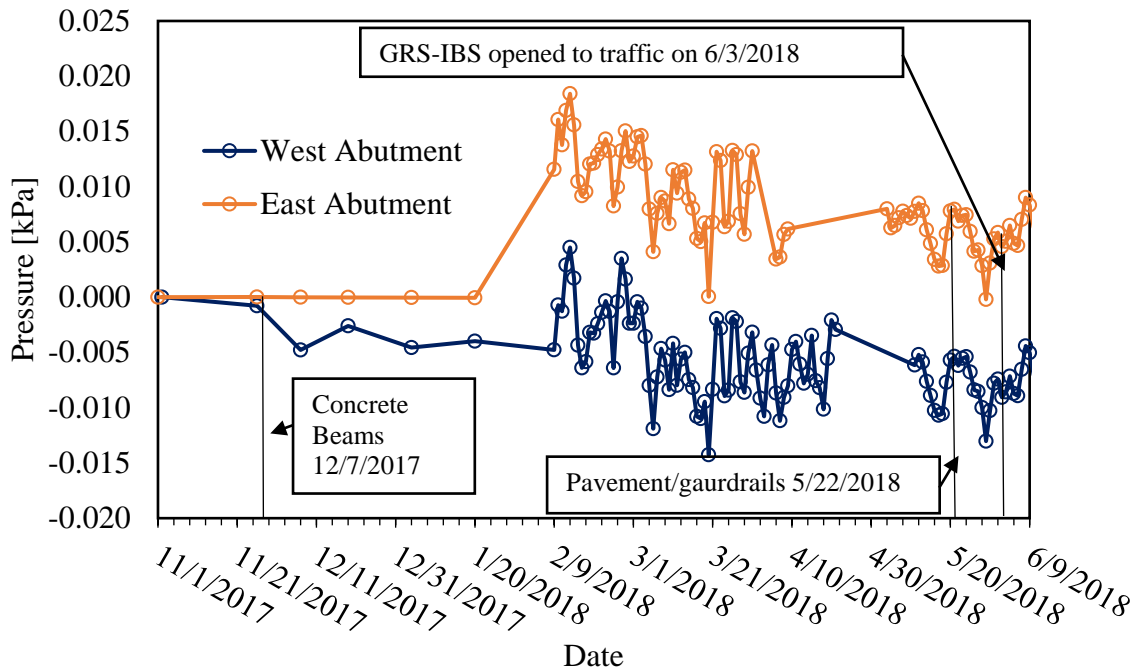


Figure 38. Pore pressure sensor readings for the east and west abutments

6.3 Geospatial Monitoring

6.3.1 Settlement

As discussed previously, periodic surveys were conducted using a total station in order to estimate any movement of the abutments relative to a fixed reference point. The survey data was collected approximately every two weeks over a period of 135 days. Little to no settlement has been recorded, as shown in Figures 39 to 41. Most of the settlement would be expected to occur immediately after construction since the abutments are constructed on hard sandstone, which is not expected to settle significantly over time. This movement was not measured since the surveys did not begin until a few weeks after the bridge beams were installed. While there are a

few outliers in the measurements in Figures 39 and 42, the majority of the data are within the estimated range of uncertainty, indicating no discernable settlement of the abutments has occurred. The uncertainty bands shown in these figures were calculated based on measurements taken from the BM at each control point. Since the BM is assumed to have a constant position, the average uncertainty was estimated by subtracting the lowest BM measurement from the highest, then dividing by two. Two control points (ECP and WCP) were used for the surveys, so two uncertainty bands were estimated. Most of the uncertainty in these measurements is likely due to errors in measuring the height of instrument (HI), which was performed using a folding measuring rule. Other sources of error include target/total station misalignment, the precision of the total station, and possible movement of the wooden power pole on which the BM was fixed. The contribution of these other factors is likely small compared to the error in measuring the HI. For example, the precision of the total station is approximately ± 0.08 in. based on the manufacturer's specifications and the error associated with surveys is approximately ± 0.2 to ± 0.4 in. between the two control points.

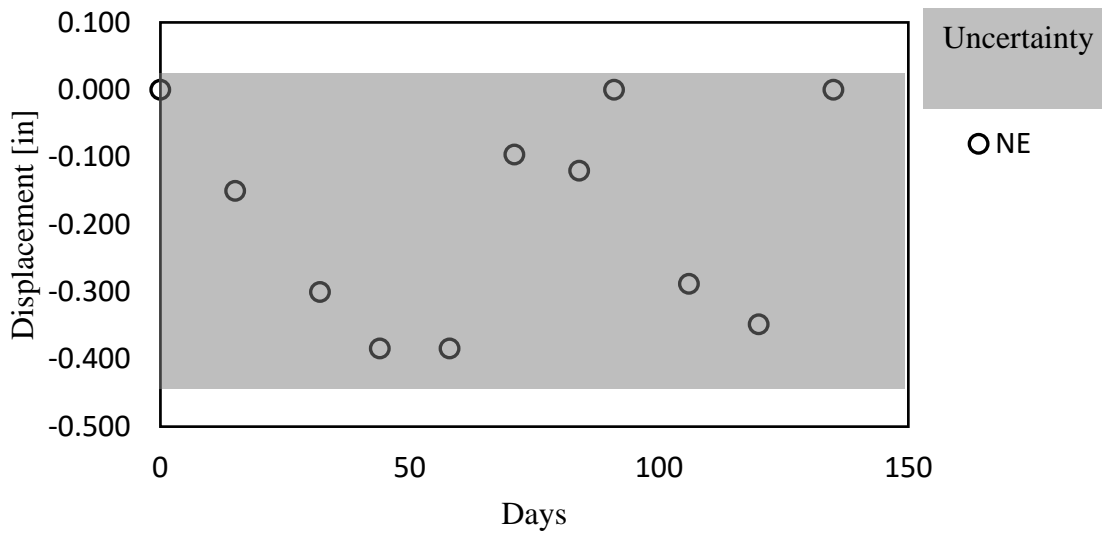


Figure 39: Settlement measurements of the northeast corner of the east abutment.

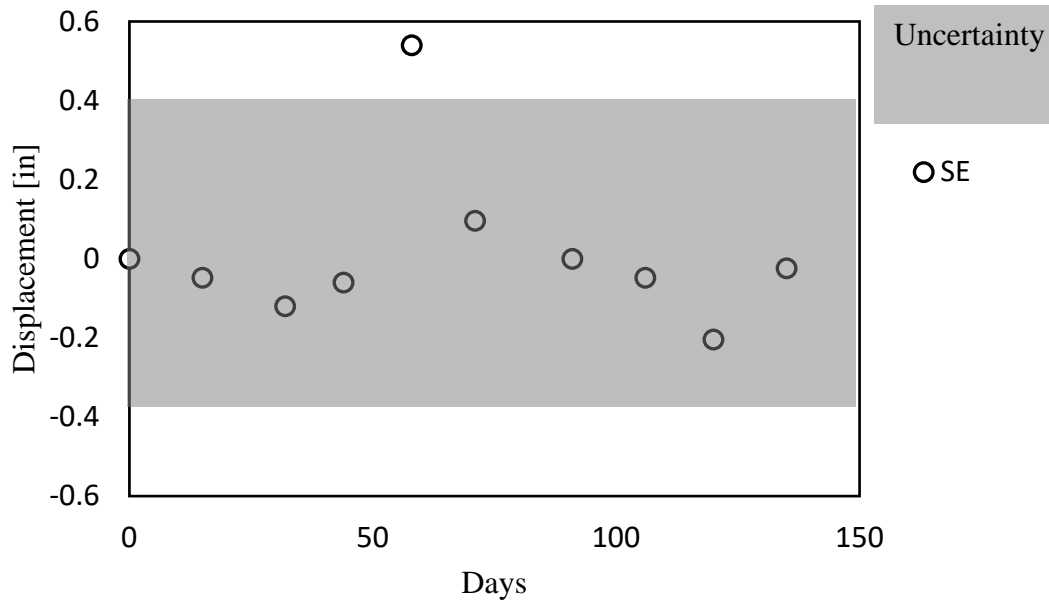


Figure 40: Settlement measurements of the southeast corner of the east abutment.

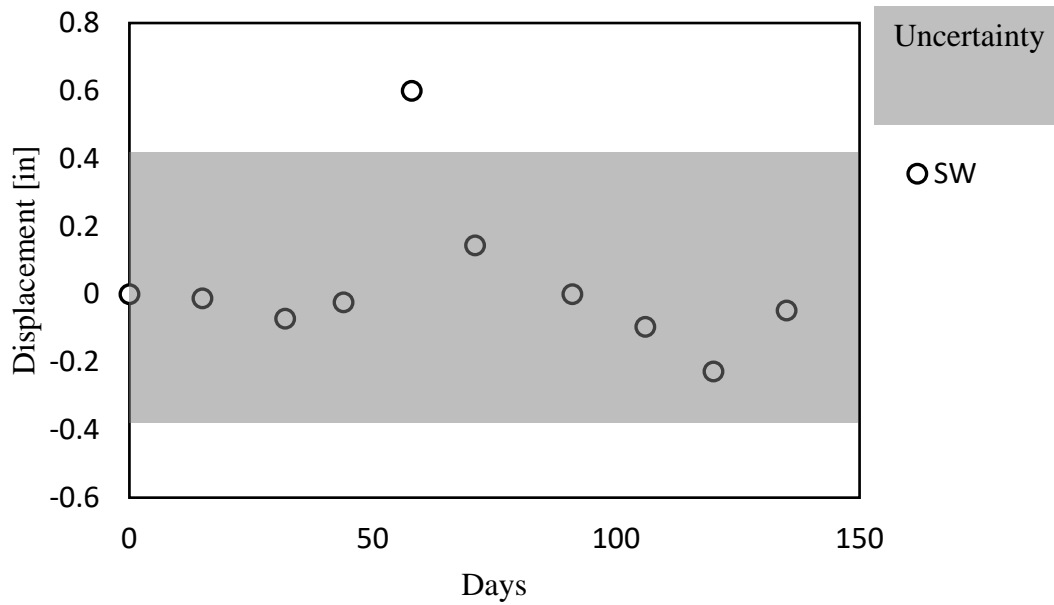


Figure 41: Settlement measurements of the southwest corner of the west abutment.

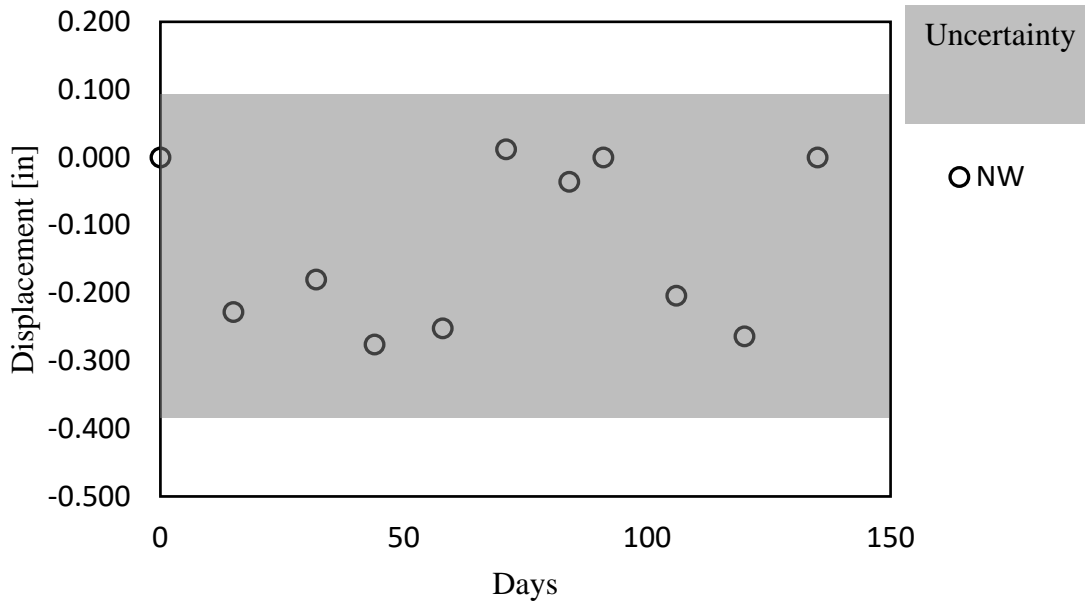


Figure 42: Settlement measurements of the northwest corner of the west abutment.

6.3.2 Lateral Displacement

The surveys have not measured any large lateral spatial movement of the abutments, indicating that the bridge is stable. The data in Figures 43-46 represent lateral displacement

measurements taken from surveys of the four outside corners of the east and west abutments. Positive lateral displacement is defined as the inward movement of the abutment (i.e., abutment to abutment movement). The uncertainty of the surveys was above the range of measured displacements in most cases; however, Figures 43, 45, and 46 display a few measurements that are above the uncertainty bands. Thermal expansion and contraction of the SRW units is the most probable cause for the displacements seen in these figures since they oscillate about zero and no discernable trend is noticed. Note that the uncertainty was calculated in a similar manner as discussed in the previous section. The Northing to the BM from each control point was assumed to be constant, therefore the uncertainty was taken as half the range between the highest and lowest values measured during the surveys.

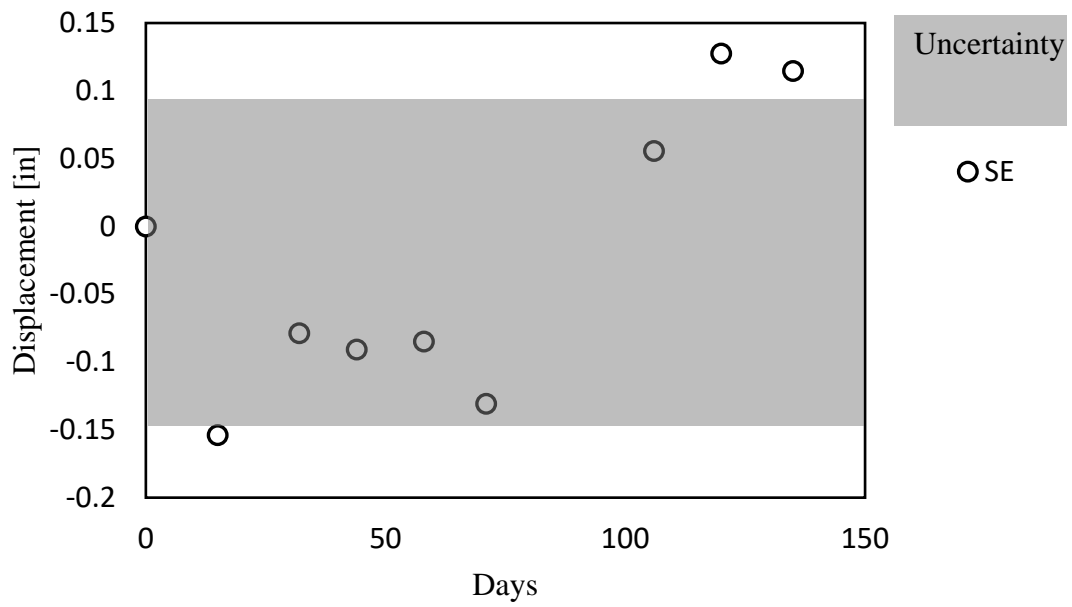


Figure 43: Measured lateral displacement of the southeast corner of the east abutment.

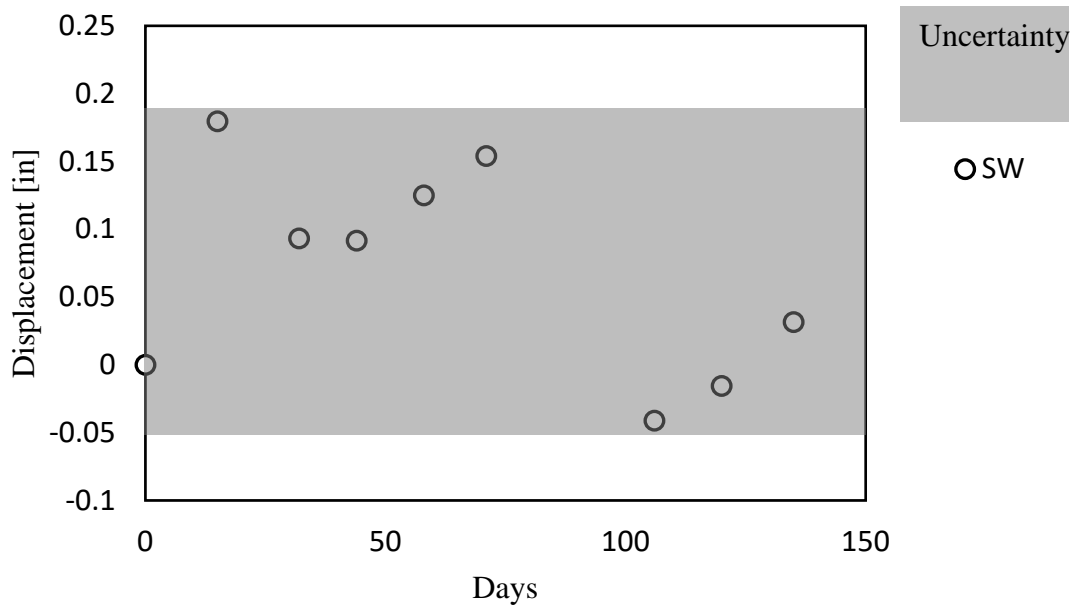


Figure 44: Measured lateral displacement of the southwest corner of the west abutment.

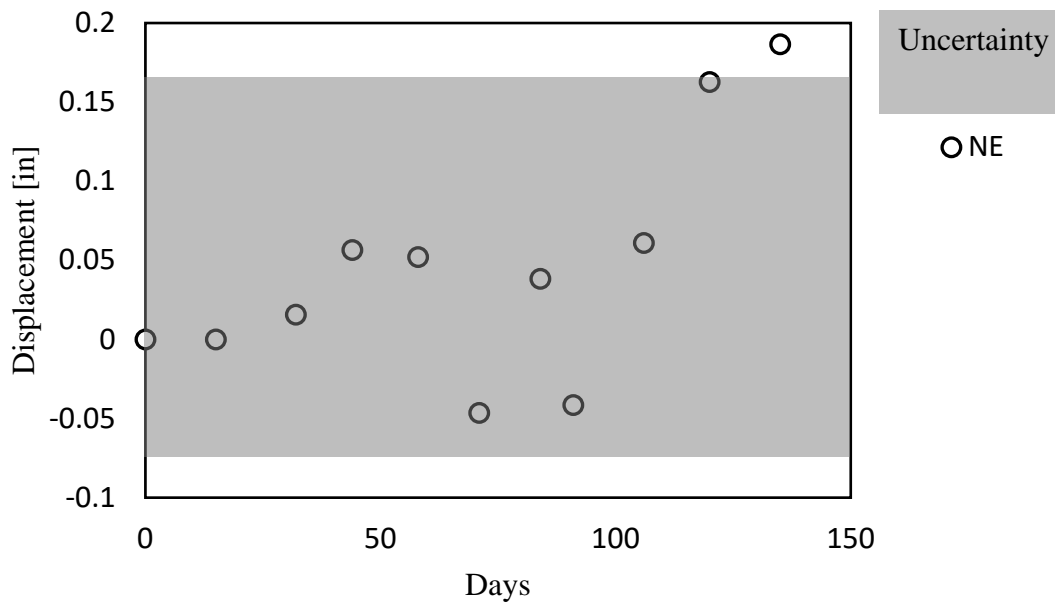


Figure 45: Measured lateral displacement of northeast corner of east abutment.

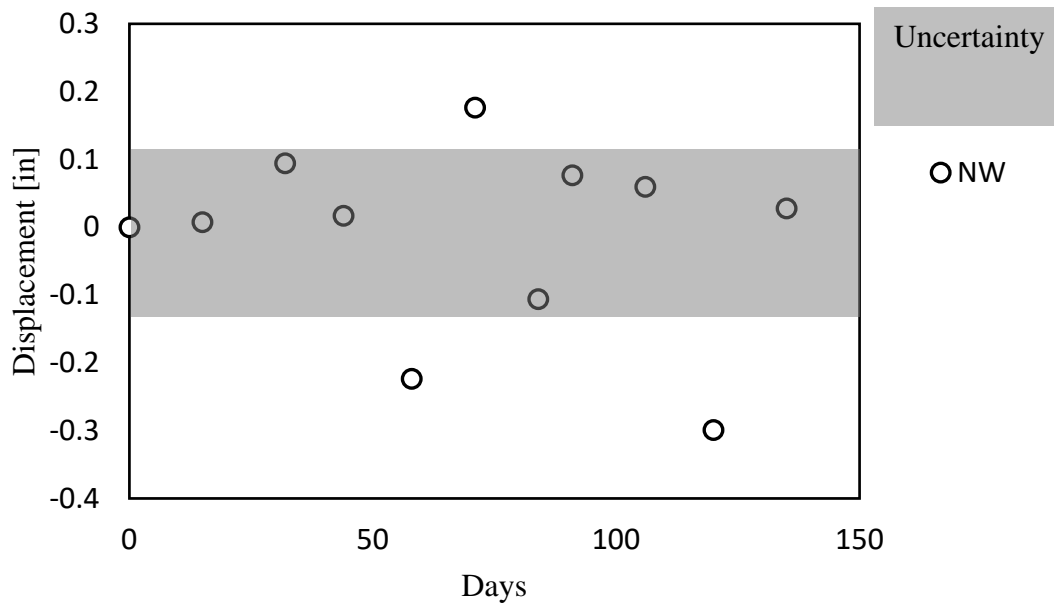


Figure 46: Measured lateral displacement of northwest corner of west abutment.

CHAPTER 7: SUMMARY, CONCLUSIONS, AND RECOMMENDATIONS

7.1 Summary of the Project

The construction of a GRS-IBS located in Albertville, AL was completed using design guidance from the FHWA (Adams et al. 2011a, b). The total project cost was about \$650,000 of which the bridge itself accounted for approximately \$317,000 with roadway construction making up the rest of the cost. The costs of each major component of the project are as follows: \$21,600 for construction of the two concrete leveling pads, \$115,600 for the GRS abutments, \$172,410 for the 7 PPC box beams, and \$7,200 for 240-lbs of structural steel (Pirando 2018). The price for the concrete leveling pads should be considered part of the GRS structure, therefore the GRS structure had a total cost of \$137,200.

Modifications to the design of the foundation were made to accommodate conditions at the Turkey Creek site. Construction proceeded with few significant issues, although delays due to weather and utility conflicts led to a longer construction period than expected. Near daily monitoring of construction by the EOR turned out to be very beneficial as issues were caught early and corrected that could have led to significant delays, and cost overruns.

7.2 Image Recording

7.2.1 Summary

All phases of construction were monitored with time-lapse cameras. The cameras have been valuable and have helped create a timeline of events that would not have been possible with site visits, since the site is many miles from the Auburn University campus. The devices were positioned to gain the best possible view as construction moved forward.

7.2.2 Conclusions

The primary goal was to create a timeline of events that would provide a clear understanding of the amount of time and effort that was invested into the construction of the GRS-IBS in Marshall County. A summary of the conclusions is provided below:

- The cameras were beneficial in keeping records of the events that took place during construction, since the GRS-IBS site was approximately 150 miles from the Auburn University campus. The cameras were set to take images at 15 and 30-min. intervals. While in most cases this is a reasonable timeframe, when construction is progressing quickly some of the details will be missed.
- To reduce the number of times a camera needs repositioning, an elevated position adjacent to the work area is the best location, although a ladder may be needed each time the memory card is removed.

7.3 Geospatial Monitoring

7.3.1 Summary

To measure settlements and movements in the horizontal plane, a surveying plan was developed. A RS60 survey target was attached to a wooden power pole located on a power pole just east of the project. This location was the common point or BM that was used for each control point, the eastern control point ECP and the western control point WCP.

7.3.2 Conclusions

Settlements and lateral displacements have been recorded so the stability of the abutments could be estimated. Conclusions that were determined are summarized below.

- While the settlement measurements that were taken are relatively precise, improvements could have been made with the use of prism type targets, since they

force the focus of the instrument to the center. The targets that were used rely on the operator to locate the center each time a survey is taken, therefore at greater distances this becomes difficult to achieve.

- When measuring the height of the instrument it is imperative to measure this value from the same location each time to ensure proper measurements are recorded. Although accurate measurements of the height of the instrument (HI) were made, systematic errors may have been introduced in the readings since the HI was not measured from the exact same location each time a survey was taken. This error likely accounts for a large portion of the uncertainty in the settlement readings. To avoid this, in addition to the center location of the control point, markings placed at the initial point, where the HI was measured from, would help to reduce the systematic error within the surveys.
- If more than one control point is used, coordinates between the two should be measured so that if one control point is ruined, the other can be used for a reference to locate and replace the missing point.
- Adams et al. (2011a) recommends using a vertical strain of 0.5 percent to determine the service stresses. Therefore, the expected vertical displacement of the Marshall County GRS-IBS is equal to 0.06 ft. The measured values in Figures 39 to 42 indicate that the abutments are well under the 0.06 ft vertical displacement calculated using 0.5 percent strain.
- Lateral movement is considered to be 2 times the vertical strain, with the maximum value located at 1/3 from the top of the GRS wall (Adams et al. 2011a). Thus, the maximum lateral displacement is located in the center of the abutment one-third of

the top. Unfortunately, no survey targets were placed at this location. However, some movement is likely to occur at the outer edges of the abutments as well. Using the previously described formulation, the maximum displacement 4 ft from the top of the abutment is 0.12 ft. The displacement at the edges of the abutment would be near zero, although small displacements are expected. Figures 43 to 46 do not show a definite trend; however, the displacements are within a tolerable range.

7.4 Instrumentation

7.4.1 Summary

Since the design a GRS structure depends largely on the horizontal stresses that develop due to loads applied at the surface as well as the weight of the backfill material. The ability to measure stresses within an abutment provides an opportunity to compare results from analytical calculations that are used to estimate design stresses.

7.4.2 Conclusions

Earth-pressure cells, and piezometers were installed in the abutments to estimate the stresses that developed due the weight of the backfill and loads applied at the surface. Conclusions from the analysis of the data are presented below.

- The earth pressure cells have provided an indication of the pressures that have developed within the abutments. According to the pressure sensor data, approximately 50 percent of the stress from the overburden is being felt by the sensor. This result is consistent with results of numerical models by Hatami and Bathurst (2005), which found an area of reduced stress behind the front of the wall due to the stiffer facing material taking on load as the backfill strains.

- The piezometers have shown that pore pressures have been and remain near zero. Once these sensors lost saturation, the readings offset from the original baseline and began to oscillate. There are a few possible reasons for this. Since the sensors have a low air entry porous stone filter, air pressure may have moved the baseline of the measurements from the initial value. Furthermore, the oscillations could possibly be due to electrical noise and changes in temperature.

7.5 Recommendations

There is a great deal of opportunity for future research into the behavior of GRS-IBS structures. The following section provides some possible avenues for future GRS-IBS research.

- Time-lapse cameras were effective for monitoring and recording the construction process. Cameras should be installed at elevated locations near the project. Since the project was many miles from the Auburn campus and construction alternated between the two abutments some details were missed. More sophisticated cameras can be used; however, two time-lapse cameras per abutment, placed at near the front and adjacent to an abutment, provided enough images to create a quality timeline of events.
- Instrumentation is valuable and can provide insight into the in-place behavior of a GRS structure. Earth-pressure cells should be used so vertical and horizontal stresses can be estimated. Piezometers should be installed at each earth pressure cell location so effective stress can be determined as well. Strain gages could also be a useful tool to measure reinforcement strains. The strains can be used to estimate the forces within the reinforcing material.

- Surveys were helpful, but skill is needed to reduce the error associated with the measurements. While the error is relatively small, the displacements of the abutments are also small, and care has to be used when using surveying techniques. Survey targets should be placed systematically on the abutments so that they can be conveniently monitored with a total station. Control points should be well marked and have a backup location, so they can be reestablished in case they are destroyed.
- Numerical models provide a way to evaluate and compare results obtained from field measurements. Once validated, numerical models can be used to evaluate other structures as well. A numerical model of the GRS-IBS in Marshall County, AL would provide a means to verify the earth pressure values that were measured with the EPC.

REFERENCES

- Adams, G.I., Butts, C., Stephenson, L.W., Cooke, W. (1926). *Geology of Alabama. Geological Survey of Alabama Special Report 14*. Tuscaloosa, Ala.: Geological Survey of Alabama.
- Adams, M., Nicks, J., Stabile, T., Wu, J., Schelatter, W. and Hartmann, J. (2011). *Geosynthetic Reinforced Soil Integrated Bridge System Interim Implementation Guide*. Publication No. FHWA-HRT-11-026, Federal Highway Administration, Washington, DC.
- Adams, M., Nicks, J., Stabile, T., Wu, J., Schelatter, W. and Hartmann, J. (2011). *Geosynthetic Reinforced Soil Integrated Bridge System Synthesis Report*. Publication No. FHWA-HRT-11-027, Federal Highway Administration, Washington, DC.
- Adams, M.T., Lillis, C.P., Wu, J.T.H., and Ketchart, K. (2002). “Vegas Mini Pier Experiment and Postulate of Zero Volume Change.” Proceedings, Seventh International Conference on Geosynthetics, pp. 389–394, Nice, France.
- Adams, M.T., Kanop, K., Wu, J.T.H. (2007). “Mini-Pier” Experiments: Geosynthetic Reinforcement Spacing and Strength as Related to Performance.” *Geosynthetics in Reinforcement and Hydraulic Applications*.
- Alabama Department of Transportation (ALDOT) (2017). Plans of Proposed Project No. BRZ-4814 (251): Marshall County Bridge Replacement and Approaches on Cochran Road at Turkey Creek with GRS-IBS. Montgomery, Alabama.
- Allen, T.M., and Bathurst, R.J. (2002). “Soil reinforcement loads in geosynthetic walls at working stress conditions.” *Geosynthetics International*, 9(5–6): 525–566.

AASHTO T-90 (2014). *Determining the Plastic Limit and Plasticity Index of Soils*, American Association of State Highway and Transportation Officials, Washington, D.C.

AASHTO T-99 (2017). *Standard Method of Test for Moisture–Density Relations of Soils Using a 2.5-kg (5.5-lb) Rammer and a 305-mm (12-in.) Drop*, American Association of State Highway and Transportation Officials, Washington, D.C.

AASHTO T-104 (1999). *Standard Method of Test for Soundness of Aggregate by Use of Sodium Sulfate or Magnesium Sulfate*, American Association of State Highway and Transportation Officials, Washington, D.C.

ASTM C140 / C140M-17b (2017) *Standard Test Methods for Sampling and Testing Concrete Masonry Units and Related Units*, ASTM International, West Conshohocken, PA

ASTM C1262 / C1262M-16 (2016). *Standard Test Method for Evaluating the Freeze-Thaw Durability of Dry-Cast Segmental Retaining Wall Units and Related Concrete Units*, ASTM International, West Conshohocken, PA, 2016,

ASTM D1238-13 (2013). *Standard Test Method for Melt Flow Rates of Thermoplastics by Extrusion Plastometer*, ASTM International, West Conshohocken, PA

ASTM C1372-17 (2017). *Standard Specification for Dry-Cast Segmental Retaining Wall Units*, ASTM International, West Conshohocken, PA

ASTM D1505-18 (2018). *Standard Test Method for Density of Plastics by the Density-Gradient Technique*, ASTM International, West Conshohocken, PA

ASTM D4439-18 (2018). *Standard Terminology for Geosynthetics*, ASTM International, West Conshohocken, PA

ASTM D4595-17 (2017). *Standard Test Method for Tensile Properties of Geotextiles by the Wide-Width Strip Method*, ASTM International, West Conshohocken, PA

ASTM D4603-18 (2018). *Standard Test Method for Determining Inherent Viscosity of Poly (Ethylene Terephthalate) (PET) by Glass Capillary Viscometer*, ASTM International, West Conshohocken, PA

ASTM D5321 / D5321M-17 (2017). *Standard Test Method for Determining the Shear Strength of Soil-Geosynthetic and Geosynthetic-Geosynthetic Interfaces by Direct Shear*, ASTM International, West Conshohocken, PA

ASTM D5819-18 (2018). *Standard Guide for Selecting Test Methods for Experimental Evaluation of Geosynthetic Durability*, ASTM International, West Conshohocken, PA

ASTM D6637 / D6637M-15 (2015). *Standard Test Method for Determining Tensile Properties of Geogrids by the Single or Multi-Rib Tensile Method*, ASTM International, West Conshohocken, PA

Barkdoll, D.B., Ettema, R., Melville, B.W. (2007). *Countermeasures to Protect Bridge Abutments from Scour.*, NCHRP Report 587., Transportation Research Board, Washington, D.C.

- Bathurst, R. J., Walters, D., Vlachopoulos, N., Burgess, P., and Allen, T. M. (2000). "Full Scale Testing of Geosynthetic Reinforced Walls." *GSP103: Advances in Transportation and Geoenvironmental Systems Using Geosynthetics*, ASCE, 201-217.
- Berg, R. R. (1991). "The Technique of Building Highway Retaining Walls," Geotechnical Fabrics Report, Industrial Fabrics Association International, St. Paul, MN, July, p38-43
- Berg, R., Christopher, B., and Samtani, N. (2009). *Design of Mechanically Stabilized Earth Walls and Reinforced Soil Slopes—Volume 1*, Report No. FHWA-NHI-10-024, National Highway Institute, Federal Highway Administration, Arlington, VA.
- Berntsen Survey Targets (2017). *RS60 Retro Reflective Survey Targets*, <www.berntsen.com> (July 2018), Berntsen International, Inc. Madison WI.
- Bloser, S., Shearer, D., Corradini, K., and Scheetz, B. (2012). "Geosynthetically Reinforced Soil Integrated Bridge Systems (GRSIBS)." Specification Development for PennDOT Publication 447, Pennsylvania Department of Transportation, Harrisburg, PA.
- Campbell Scientific (2017). *Instruction Manual—Model CRVW3 Data Logger*, Campbell Scientific, Inc., Logan UT.
- Clyne, T.R., (2011). "Monitoring Geosynthetics in Local Roadways: 10-Year Performance Study." Minnesota Department of Transportation. St. Paul, MN.
- Daniyarov, A., Zelenko, B., Derian, A. (2017). *Deployment of the Geosynthetic Reinforced Soil Integrated Bridge System From 2011 to 2017*, Report No. FHWA-HIF-17-043, Federal Highway Administration, Washington, D.C.
- Elton, D.J. (2014). "GRS-IBS Implementation Assistance and Monitoring" Highway Research Center, Auburn University, Auburn, AL.

- Geokon (2009). Instruction Manual – Model 4500 Series Vibrating Wire Piezometers, Geokon, Inc, Lebanon, NH.
- Geokon (2010). *Instruction Manual – Models 4800, 4810, 4815, 4820, and 4830 VW Earth Pressure Cells*, Geokon, Inc, Lebanon, NH.
- Ghazvinei, P.T., Ariffin, J., Abdullah, J. Mohammad, T.A., (2014). “Assesment of Local Scour at Bridges Abutment” *Research Journal of Applied Sciences, Engineering and Technology*.
- Grubb, M. A., P.E., Wilson, K. E., P.E., S.E., White, C. D., P.E., Nickas, W. N, P.E. (2007, 2015). *Load and Resistance Factor Design (LRFD) For Highway Bridge Superstructures-Reference Manual*, Report No. FHWA-NHI-15-047, Federal Highway Administration National Highway Institute (HNHI-10) Arlington, VA.
- Hatami, K., and Bathurst, R. J. (2005). “Development and verification of a numerical model for the analysis of geosynthetic-reinforced soil segmental walls under working stress conditions.” *Canadian Geotechnical Journal*, 42(4), 1066–1085.
- Holtz, R. D., Barry R. Christopher, and Ryan R. Berg (2008). *Geosynthetic Design & Construction Guidelines: Reference Manual*, U.S. Dept. of Transportation, Federal Highway Administration, National Highway Institute
- igeosynthetics (2017). *Image of roll geosynthetic material with directional indicators as manufactured*. <<http://www.igeosynthetics.com>> (July 7, 2018)
- Ingold, T. S. (1994). “The Geotextiles and Geomembranes Handbook.” 1st ed. Oxford, UK: Elsevier Advanced Technology.

- Koerner, R. M. (2012). "Designing with Geosynthetics." 6th ed. Upper Saddle River, NJ: Prentice Hall.
- Kulicki, J. M., and Mertz, D. (2006). "Evolution of vehicular live load models during the interstate design era and beyond." 50 Years of Interstate Structures: Past, Present and Future. Transportation Research Circular No. E-C104, Transportation Research Board (TRB), Washington, DC.
- Meehan, C. L., and Poggiogalle, T. M. (2017). *Long Term Monitoring of a Geosynthetic Reinforced Soil Integrated Bridge System (GRS-IBS): Final Report*. Center for Advanced Infrastructure and Transportation, Rutgers, The State University of New Jersey, Piscataway, NJ.
- Neilson, M. (2007). "Cumberland Plateau Physiographic Section" Encyclopedia of Alabama <<http://www.encyclopediaofalabama.org/article/h-1301>> (Jun. 20, 2018).
- Nicks, J., Adams, M., (2013). *Friction Angles of Open-Graded Aggregates from Large Scale Direct Shear Testing*, Publication No. FHWA-HRT-13-068, Federal Highway Administration, Washington, DC.
- Nicks, J.E., Adams, M.T., Ooi, P.S.K., Stabile, T. (2013). *Geosynthetic Performance Soil Testing—Axial Load Deformation Relationships*, Report No. FHWA-HRT-13-066, Federal Highway Administration, Mclean, VA.
- Peavy, T. (2008). Provenance of Lower Pennsylvanian Pottsville Formation, Cahaba Synclinorium. Thesis, Auburn University, Auburn, Alabama.
- Pirando, R., P.E. (2018) personal communication through email

- Pomeroy, J.S., Thomas, R.E. (1985). "Geologic Relationships of Slope Movement in Northern Alabama." U.S. Geological Survey Bulletin 1649, United States Geologic Survey Alexandria, VA.
- Saghebfar, M., Abu-Farsakh, M., Ardah, A., Chen, Q., and Fernandez, B. A. (2017). "Performance monitoring of Geosynthetic Reinforced Soil Integrated Bridge System (GRS-IBS) in Louisiana." *Geotextiles and Geomembranes*, 45(2), 34–47.
- Shukla, S. K. (2002) "Geosynthetics and Their Applications." London: Thomas Telford.
- SIG Testing Services (2017). Wide-Width Tensile Testing (ASTM D 4595) US 4800 Woven Geotextile. SIG Lab Sample ID S20528, Project No. SIG12026. N-ocross, Georgia.
- S&ME (2017). Testing of Segmental Retaining Wall Units. Job No. 1803-10-183, Report No. 001017. Duluth, Georgia.
- Steward, J.E. and Mohny, J. (1982). "Trial Use Results and Experience for Low Volume Forest Roads," Proceedings, 2nd International Conference on Geotextiles, Las Vegas, Vol. II, pp. 335-340.
- Turnbull, W.S. Jr., (2014). "Geosynthetically Reinforced Soil Bridge Abutments." Master of Civil Engineering Project, Auburn University, Auburn AL.
- Vennapusa, P., White, D., Klaiber, W., Wang, S. (2012). *Geosynthetic Reinforced Soil for Low-Volume Bridge Abutments: Final Report*. Iowa Highway Research Board, Iowa Department of Transportation, Ames Iowa.
- White, D.J., Vennapusa, P., Klaiber, W. (2012). *Geosynthetic Reinforced Soil for Low-Volume Bridge Abutments: Tech Transfer Summary*. Iowa Highway Research Board (IHRB Project TR-621), Iowa Department of Transportation, Ames Iowa.

- Wingscapes (2017). *TimelapseCam Camera*. < www.wingscapes.com > (July 24, 2018) Ebsco Industries, Inc. Birmingham, AL.
- Wrigley, N. E. (1987). Durability and Long-Term Performance of ‘Tensar’ Polymer Grids for Soil Reinforcement, *Materials Science and Technology*, Vol. 3, p161-170
- Wu, J.T.H. (1994). *Design and Construction of Low Cost Retaining Walls: The Next Generation in Technology*, Report No. CTI-UCD-1-94, Colorado Transportation Institute, Denver, CO
- Wu, J.T.H., Lee, K.Z.Z., Helwany, S.B., and Ketchart, K. (2006). *Design and Construction Guidelines for GRS Bridge Abutment with a Flexible Facing*, Report No. 556, National Cooperative Highway Research Program, Washington, DC.
- Wu, J.T.H., Pham, T.Q., and Adams, M.T. (2013). *Composite Behavior of Geosynthetic-Reinforced Soil Mass*, Federal Highway Administration, McLean, VA.
- Wu, J.T.H, Ooi, P.S.K. (2015). *Synthesis of Geosynthetic Reinforced Soil Design Topics*, Report No. FHWA-HRT-14-094, Federal Highway Administration, Mclean, VA
- Zornberg, J.G. (2014). “Advances in the Use of Geosynthetic-reinforced Soil Structures,” Proceedings of the 14th National Congress on Geotechnics, Portuguese Geotechnical Society, Covilha, Portugal, 06-09 April, pp. 11-3